

**EQUILIBRIUM FORESHORE SLOPE AND CROSS-SHORE  
SEDIMENT TRANSPORT VALIDATED THROUGH LABORATORY  
EXPERIMENTS AND FIELD DATA ANALYSIS**

by

JIRAT LAKSANALAMAI AND NOBUHISA KOBAYASHI

RESEARCH REPORT NO. CACR-24-01  
January 2024



CENTER FOR APPLIED COASTAL RESEARCH  
University of Delaware  
Newark, Delaware 19716

## **ACKNOWLEDGMENTS**

The data for the analysis of the Pattaya beach nourishment project in this study was made available by various organizations in Thailand: the Marine Department of Ministry of Transport; the Aquatic Resources Research Institute at Chulalongkorn University; and Aurora Technology and Engineering Consultant Co., Ltd. The first author received support from the Office of the Civil Service Commission under the Government of Thailand during his studies at the Center for Applied Coastal Research at University of Delaware, Newark, Delaware.

## TABLE OF CONTENTS

LIST OF TABLES .....	4
LIST OF FIGURES .....	6
ABSTRACT .....	8
1 INTRODUCTION .....	9
2 WAVE FLUME EXPERIMENT .....	11
2.1 Wave Flume, Sand Beach, and Instruments .....	11
2.2 Data Analysis.....	16
3 ANALYTICAL MODEL .....	24
4 LABORATORY DATA COMPARISON .....	27
5 PATTAYA BEACH.....	32
6 FIELD DATA COMPARISON .....	49
7 CONCLUSIONS .....	56
REFERENCES .....	58
APPENDIX .....	61

## LIST OF TABLES

Table 2.1	Wave gauge locations (WG1-WG8) and velocimeter locations (ADV; Red Vectrino, RV; and Blue Vectrino, BV).....	13
Table 2.2	Sequence of three tests consisting of 100 runs, with each run lasting 400s. ....	14
Table 6.1	Equilibrium foreshore slope model parameters for the laboratory beach and Pattaya beach.....	52
Table A.1	Incident wave characteristics, Test E1-E20 .....	62
Table A.2	Incident wave characteristics, Test S1-S20.....	63
Table A.3	Incident wave characteristics, Test M1-M60 .....	64
Table A.4	Mean free-surface elevation $\bar{\eta}$ (cm) at 8 wave gauge locations, Test E1-E20.....	67
Table A.5	Mean free-surface elevation $\bar{\eta}$ (cm) at 8 wave gauge locations, Test S1-S20 .....	68
Table A.6	Mean free-surface elevation $\bar{\eta}$ (cm) at 8 wave gauge locations, Test M1-M60.....	69
Table A.7	Free-surface standard deviation $\sigma_{\eta}$ (cm) at 8 wave gauge locations, Test E1-E20 .....	72
Table A.8	Free-surface standard deviation $\sigma_{\eta}$ (cm) at 8 wave gauge locations, Test S1-S20.....	73
Table A.9	Free-surface standard deviation $\sigma_{\eta}$ (cm) at 8 wave gauge locations, Test M1-M60.....	74
Table A.10	Mean $\bar{U}$ and standard deviation $\sigma_U$ of measured cross-shore velocity $U$ , Test E1-E20.....	77

Table A.11	Mean $\bar{U}$ and standard deviation $\sigma_U$ of measured cross-shore velocity $U$ , Test S1-S20.....	78
Table A.12	Mean $\bar{U}$ and standard deviation $\sigma_U$ of measured cross-shore velocity $U$ , Test M1-M60.....	79

## LIST OF FIGURES

Figure 2.1	Experimental setup at the start of equilibrium foreshore slope test. ....	12
Figure 2.2	Experimental setup: beach profile, wave gauges, and velocimeters. ....	14
Figure 2.3	Initial profiles E0, S0, and M0 for Equilibrium, Steep, and Mild slope tests. ....	15
Figure 2.4	Average values of mean and standard deviation of free surface elevation $\eta$ and cross-shore velocity $U$ for 20 or 60 runs in tests E, S, and M. ....	17
Figure 2.5	Measured profiles E0, E10, and E20 and cross-shore sand transport rate $\bar{q}_x$ during the intervals of E0-E10 and E10-E20. ....	20
Figure 2.6	Measured profiles S0, S10, and S20 and cross-shore sand transport rate $\bar{q}_x$ during the intervals of S0-S10 and S10-S20. ....	21
Figure 2.7	Measured profiles M0, M10, M20, M30, M40, M50, and M60 and cross-shore sand transport rate $\bar{q}_x$ during the six intervals from M0-M10 to M50-M60. ....	22
Figure 4.1	Analytical equilibrium profile model fitted to measured equilibrium profile E10 where the toe depth $h_t$ , profile scale factor $A$ , and swash slope $S_s$ are input to the model. ....	28
Figure 4.2	Analytical sand transport rate $q_x$ predicted for each of the measured profiles of E10 and E20 in comparison to average rate $\bar{q}_x$ during the interval of E10-E20. ....	29
Figure 4.3	Analytical sand transport rate $q_x$ predicted for each of the measured profiles of S0 and S10 in comparison to average rate $\bar{q}_x$ during the interval of S0-S10. ....	30
Figure 4.4	Analytical sand transport rate $q_x$ predicted for each of the measured profiles of M0 and M10 in comparison to average rate $\bar{q}_x$ during the interval of M0-M10. ....	31
Figure 5.1	Pattaya beach location in Thailand (ArcGIS Pro). ....	33

Figure 5.2	Pattaya beach (Google earth Pro) on October 22, 2022 after the sand placement (130 m <sup>3</sup> /m) between the south and north groins constructed in 2018. ....	34
Figure 5.3	Pattaya beach during 2019-2023 after sand placement. ....	36
Figure 5.4	Thirty cross-shore lines (L1-L30) and four zones (SL, SS, NL, and NS) for the sand volume changes during 2015-2023. ....	37
Figure 5.5	Measured profile changes (L2-L30) in 2015, 2019, 2020, 2021, 2022, and 2023. ....	46
Figure 5.6.	Alongshore averaged profiles in the south zones of SS and SL in 2015, 2019, 2020, 2021, 2022, and 2023. ....	47
Figure 5.7	Alongshore averaged profiles in the north zones of NS and NL in 2015, 2019, 2020, 2021, 2022, and 2023. ....	48
Figure 6.1	Annual cross-shore sand transport rate $\overline{q_x}$ for the four intervals (2019-2023) estimated using alongshore averaged profiles in the south zones (SS and SL) and assuming alongshore uniformity. ....	50
Figure 6.2	Annual cross-shore sand transport rate $\overline{q_x}$ for the four intervals (2019-2023) estimated using alongshore averaged profiles in the north zones (NS and NL). ....	51
Figure 6.3	Estimation of model parameters $h_t$ , $A$ , and $S_s$ for the SL zone, and comparison of measured sand transport rate $\overline{q_x}$ and average analytical rate $q_x$ during 2019-2020 and 2022-2023. ....	54
Figure 6.4	Estimation of $h_t$ , $A$ , and $S_s$ for the NL and NS zone, and comparison of measured sand transport rate $\overline{q_x}$ and average analytical rate $q_x$ during 2019-2020 and 2022-2023. ....	55

## ABSTRACT

In countries where coastal engineering is developing, there is growing tendency to employ beach nourishment as coastal protection, despite limited wave data. This study introduces a simple analytical model proposed to estimate cross-shore sediment transport on a measured beach profile when wave data is unavailable. The model predicts offshore (onshore) sediment transport on the foreshore slope which is steeper (milder) than the equilibrium foreshore slope. A wave flume experiment was conducted to assess the model. Equilibrium, steep, and mild foreshores were constructed on a beach consisting of fine sand and exposed to identical irregular waves. The steep foreshore experienced rapid erosion, quickly transitioning to equilibrium, while accretion and equilibration on the mild slope occurred gradually.

The calibrated model is able to predict the sediment transport rates on both the initial steep and mild foreshores with clear deviations from the equilibrium foreshore profile. The analytical model is furthermore compared with the nourished beach data at Pattaya, Thailand. Over the period from 2019 to 2023, bathymetric and topographic measurements were conducted yearly but water level and wave data were not measured. The analyzed sand volume changes and beach profile changes in the area of the sand placement were founded to be surprisingly small. The analytical model is subsequently used to interpret the cross-shore sediment transport rate per unit width of the order of  $10 \text{ m}^2/\text{y}$ .

## Chapter 1

### **INTRODUCTION**

Our understanding and predictive capabilities of cross-shore sediment transport processes have improved with the increased availability of laboratory and field data as reviewed in the Coastal Engineering Manual (USACE 2003). Kobayashi (2016) assessed the capabilities and limitations of more recent process-based models used for engineering applications. The prediction of long-term beach profile evolution using such models is still challenging because small errors tend to accumulate in the long-term simulation. Moreover, profile prediction models require water level and wave data for the duration of the profile prediction. Continuous wave data is frequently unavailable in countries where coastal engineering is still in the development phase (Laksanalamai and Kobayashi 2021). While bathymetry and topography surveys are normally conducted for coastal engineering projects, the absence of wave data poses a significant obstacle to accurate predictions. In response, this study attempts to predict the cross-shore sediment transport rate on the surveyed beach profile despite the unavailability of wave data.

The equilibrium beach profile model of Dean (1991) does not require wave data apart from the estimation of the seaward limit (closure depth) of the equilibrium profile. The net cross-shore sediment transport rate is presumed to be zero. The sediment transport direction (onshore or offshore) has been predicted separately using

dimensionless parameters based on the sediment and wave characteristics as reviewed in the textbook of Dean and Dalrymple (2002). Offshore sediment transport associated with dune erosion during a storm was assumed to be proportional to the difference between the actual and equilibrium wave energy dissipation per unit volume by Kriebel and Dean (1985). Kobayashi (1987) reformulated this offshore transport equation in relation to the still water depth and local bottom slope below the increased water level during a storm. The rewritten formula elucidates the increased offshore sediment transport on the steep dune slope. No succinct formula existed for the empirical prediction of onshore sediment transport. The long-term beach profile simulation involves both erosion and accretion.

This study introduces the concept of an equilibrium foreshore slope. Cross-shore sediment transport is offshore (onshore) when the actual foreshore exhibits a steeper (milder) slope than the equilibrium slope. The hypothesis is confirmed in a wave flume experiment in which equilibrium, steep, and mild foreshores consisting of the same sand were subjected to almost identical irregular breaking waves. The analytical model for the cross-shore sediment transport by Kobayashi et al. (2018) is rearranged to highlight the equilibrium foreshore slope and compared with the experimental data. Subsequently, the validated model is tested using yearly bathymetry and topography data of Pattaya beach in Thailand, a beach characterized by limited availability of water level and wave data (Laksanalamai and Kobayashi 2021).

## Chapter 2

### WAVE FLUME EXPERIMENT

The laboratory experiment was conducted to measure the beach profile change of equilibrium, steep, and mild slope foreshores. This chapter provides an overview of the experiment in a wave flume located in the basement of the Dupont Hall of the University of Delaware.

#### 2.1 Wave Flume, Sand Beach, and Instruments

An experiment was conducted in a wave flume that was 23 m long, 1.15 m wide, and 1.5 m high, as shown in Fig. 2.1, for the first equilibrium (E) foreshore slope test. The experimental setup was based on the previous equilibrium profile tests conducted by Laksanalamai and Kobayashi (2023) who tracked small objects (gravel and microplastics) on the equilibrium beach. The sand beach on a plywood slope of 1/30 (vertical/ horizontal) consisted of well-sorted sand with a median diameter of 0.18 mm and a fall velocity of 2.0 cm/s. A 400-s run of irregular waves with a Texel, Marsen, and Arsloe (TMA) spectrum was generated by a piston-type wave maker in a water depth of 0.88 m. The input signal for the wave generation was kept the same. The significant wave height and peak period were 0.2 m and 2.6 s. A vertical wall was located at the landward edge of the sand beach. The wall crest elevation was 0.2 m above the still water level (SWL) in the wave flume. No wave overtopping and overwash of

the wall occurred because of no sand in the trap and no water in the collection basin in this experiment.

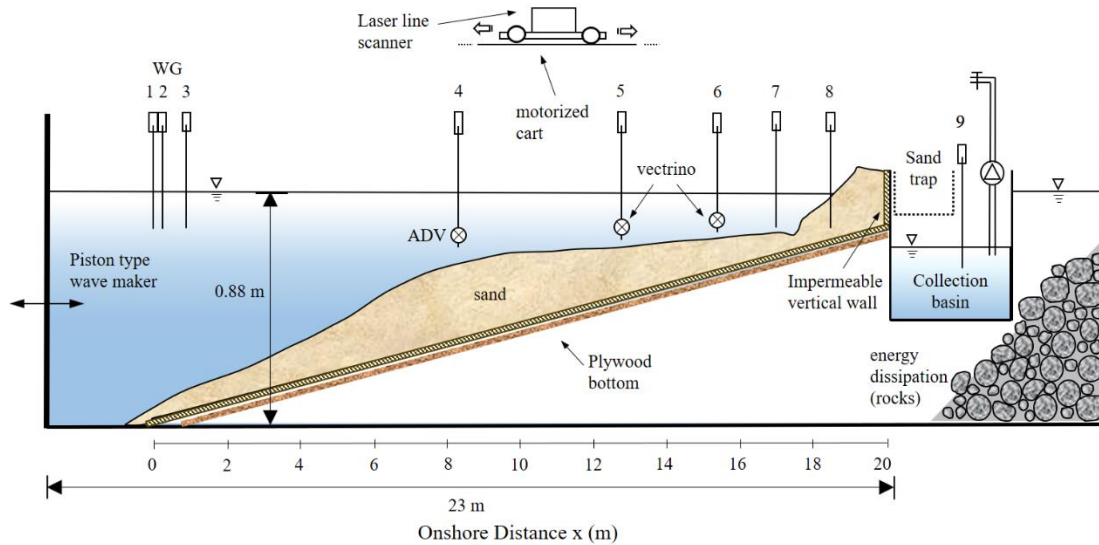


Figure 2.1 Experimental setup at the start of equilibrium foreshore slope test.

Eight wave gauges (WG1-WG8) were used to measure the free surface in the shoaling, surf, and swash zones. The fluid velocities were measured by one acoustic Doppler velocimeter (ADV) and two Vectrino (NorTek, Rud, Norway) acoustic velocimeters at an elevation above the bed of one-third of the local water depth. All wave gauges and velocimeters locations are listed in Table 2.1. Beach profile and experimental setup are shown in Fig. 2.2. The vertical wall was located at the onshore distance  $x$  of 19.9 m with  $x = 0$  at WG1. The vertical coordinate  $z$  is positive upward with  $z = 0$  at the SWL. The beach profile was measured using a laser line scanner system mounted on a motorized cart. The laser scanner recorded a longshore transect across the flume width at 2-cm cross-shore intervals after the water level was lowered for the

survey. Three-dimensional bathymetry data were averaged alongshore to obtain the alongshore-averaged beach profile.

Table 2.1 Wave gauge locations (WG1-WG8) and velocimeter locations (ADV; Red Vectrino, RV; and Blue Vectrino, BV)

Wave Gauge	WG1	WG2	WG3	WG4	WG5	WG6	WG7	WG8
$x$ (m)	0.00	0.25	0.95	8.30	12.90	15.50	17.10	18.60
$y$ (m)	0.00	0.00	0.00	0.00	0.00	0.00	0.00	0.00
Velocity Gauge				ADV	RV	BV		
$x$ (m)				8.30	12.90	15.50		
$y$ (m)				0.15	0.15	0.00		
$z$ (m)				$-2d/3$	$-2d/3$	$-2d/3$		

$d$  = local water depth

$x$  = onshore coordinate with  $x = 0$  at WG1

$y$  = alongshore coordinate with  $y = 0$  at the middle of the wave flume

$z$  = vertical coordinate with  $z = 0$  at SWL

The sequence of three tests in the experiment is summarized in Table 2.2. The E, S, and M tests correspond to the equilibrium, steep, and mild foreshore slopes, respectively. The initial profile E0 was measured at the start of the E test where the numeral after the letter E corresponds to the run number starting from zero. The profiles were measured every ten runs. The profiles of E0, E10, and E20 were compared to confirm negligible profile changes (less than 5 mm) during the 20 runs lasting 8,000 s. After E20, the foreshore profile was modified manually to create a steeper foreshore for the initial profile S0. The total sand volume was kept the same.



Figure 2.2 Experimental setup: beach profile, wave gauges, and velocimeters.

Table 2.2 Sequence of three tests consisting of 100 runs, with each run lasting 400s.

Test	Slope	Run number of profile measurement
E	Equilibrium	E0, E10, and E20
S	Steep	S0, S10, and S20
M	Mild	M0, M10, M20, M30, M40, M50, and M60

Fig. 2.3 compares the initial profiles E0 and S0 where the foreshore slope was increased from about 0.2 for E0 to 0.3 for S0. The steep foreshore was eroded rapidly during 10 runs and the measured profile S10 was similar to the equilibrium profile E0. Additional 10 runs were conducted to confirm negligible profile changes from S10 to S20. The mild foreshore slope of about 0.1 for the initial profile M0 (Fig. 2.3) was created by moving sand offshore. The mild foreshore evolved slowly toward the equilibrium profile E0 from M0 to M60. The M test was terminated after 60 runs because of the slow asymptotic approach. It is noted that the bottom elevation changes were negligible in the zone of  $x < 15$  m in Fig. 2.3 because the experiment was started from the equilibrium beach profile under the same wave conditions.

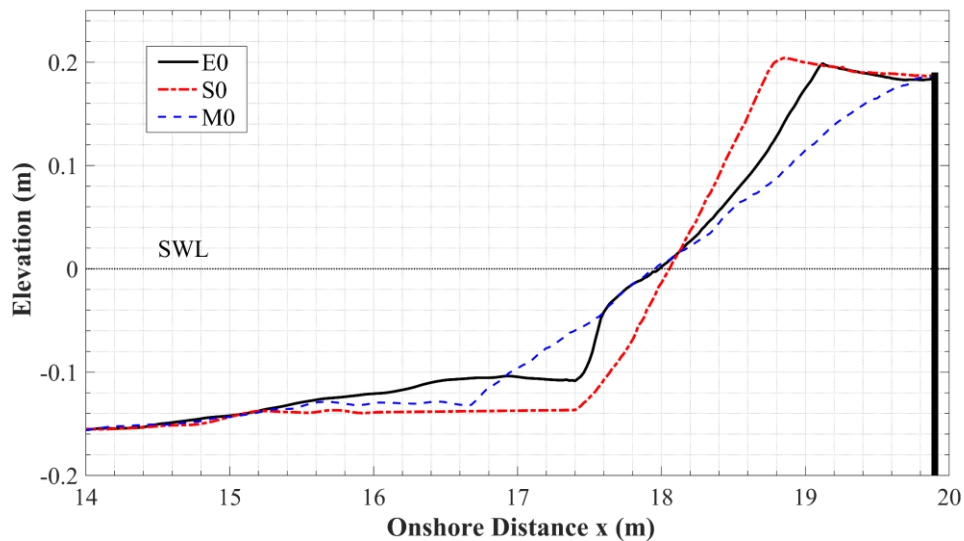


Figure 2.3 Initial profiles E0, S0, and M0 for Equilibrium, Steep, and Mild slope tests.

## 2.2 Data Analysis

The time series obtained by the eight wave gauges and three velocimeters in Fig. 2.1 were analyzed for each of the 100 runs. The incident and reflected waves were estimated using WG1, WG2, and WG3 at  $x = 0.0$ ,  $0.25$ , and  $0.95$  m, respectively. The method based on linear wave theory summarized by Goda (2010) was used to separate the incident and reflected waves outside the surf zone. The spectral significant wave height  $H_{mo}$  and peak period  $T_p$  of the incident waves at  $x = 0.0$  were  $0.2$  m and  $2.6$  s, respectively. The wave reflection coefficient was defined as the ratio between the values of  $H_{mo}$  for the reflected and incident waves. The reflection coefficient was  $0.16$  for the equilibrium foreshore slope of E1-E20 and approached to  $0.16$  during the S and M tests where the reflection coefficient decreased (increased) by  $0.02$  with the foreshore slope decreased (increased) from S1 (M1) to S20 (M60).

The irregular wave shoaling and breaking was measured by WG4 ( $x = 8.3$  m) and WG5 ( $x = 12.9$  m) in the outer surf zone. Broken waves in the inner surf zone were measured by WG6 ( $x = 15.5$  m) and WG7 ( $x = 17.1$  m) in the zone of gentle bottom slope seaward of the steeper swash zone in Fig. 2.3. WG8 ( $x = 18.6$  m) was in the swash zone of noticeable bottom elevation changes in the S and M tests. The velocities were measured at  $x = 8.3$ ,  $12.9$ , and  $15.5$  m. The measured alongshore and vertical velocities were small in comparison to the cross-shore velocity  $U$ . The mean and standard deviation of the free surface elevation  $\eta$  and horizontal velocity  $U$  for each of the 100 runs were calculated and tabulated for each of the eight wave gauges and three velocimeters in Appendix. The calculated values in each test are averaged and plotted

in Fig. 2.4 where the number of runs was 20, 20, and 60 for the E, S, and M tests, respectively.

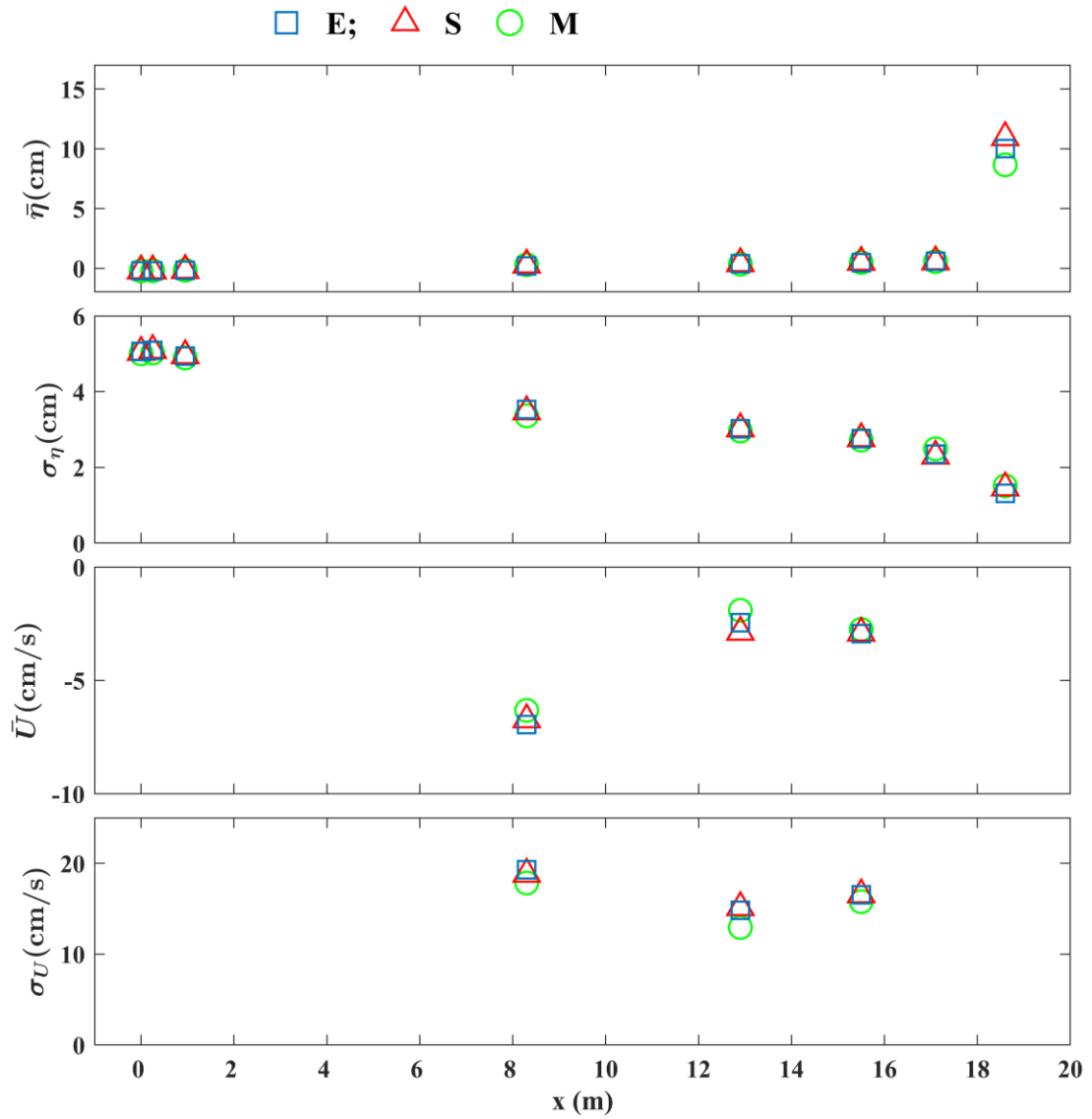


Figure 2.4 Average values of mean and standard deviation of free surface elevation  $\eta$  and cross-shore velocity  $U$  for 20 or 60 runs in tests E, S, and M.

The mean water level  $\bar{\eta}$  in Fig. 2.4 was slightly negative (-0.2 cm) for WG1-WG3 outside the surf zone for the three tests. The positive  $\bar{\eta}$  (wave setup) for WG4-WG7 increased landward and was approximately 0.6 cm at WG7. The value of  $\bar{\eta}$  at WG8 above the SWL was the sum of the mean depth and the sand surface elevation at WG8. The values of  $\bar{\eta}$  at WG8 were about 10 cm for E1-E20, decreased from 15 cm to 10 cm during S1-S20, and remained about 9 cm during M1-M60. The average value of  $\bar{\eta}$  at WG8 was 10.0, 10.9, and 8.7 cm for the E, S, and M tests, respectively. The free surface standard deviation  $\sigma_{\eta}$  is related to the local significant wave height  $H_{mo} = 4\sigma_{\eta}$ . The values of  $\sigma_{\eta}$  were approximately 5 cm at WG1-WG3 and decreased from about 3.4 cm at WG4 to about 1.4 cm at WG8. The average offshore current ( $-\bar{U}$ ) was about 7 cm/s at  $x = 8.3$  m and 2-3 cm/s at  $x = 12.9$  and 15.5 m. The corresponding value of  $\sigma_U$  was about 19 cm/s at  $x = 8.3$  m and 13-16 cm/s at  $x = 12.9$  and 15.5 m.

The hydrodynamic conditions seaward of the foreshore slopes in Fig. 2.3 were similar for the E, S, and M tests. The differences of the profile evolutions among the three tests must have been caused mostly by the initial profile differences. The Dean number  $D$  and the profile parameter  $P$  (Dalrymple 1992) have been used to predict the cross-shore sediment transport direction. The incident waves may be represented by  $H_{mo} = 0.2$  m and  $T_p = 2.6$  s at WG1. The sediment is characterized by the fall velocity  $w = 0.02$  m/s. The values of  $D = H_{mo}/wT_p$  and  $P = gH_{mo}^2/(w^3T_p)$  with  $g =$  gravitational acceleration are 3.8 and 19,000 in this experiment. These values may indicate the borderline between erosion (offshore) and accretion (onshore) in view of different

criteria given by Dean and Dalrymple (2002). The beach profile in the zone of  $x < 15$  m in Fig. 2.3 was stable in this experiment. However, the criteria based on  $D$  and  $P$  with no foreshore slope cannot explain the foreshore erosion (accretion) in the S (M) test.

Fig. 2.5 shows the measured profiles E0, E10, and E20 in the equilibrium profile test. The step at the toe of the foreshore was stable at the location of wave uprush and downrush collision in the lower swash zone. The cross-shore sand transport rate  $q_x$  per unit width is positive onshore and estimated using the measured bottom elevation  $Z_b$  and the continuity equation of bottom sediment

$$(1 - n_p) \frac{\partial Z_b}{\partial t} + \frac{\partial q_x}{\partial x} = 0 \quad (1)$$

where  $t$  = morphological time;  $x$  = onshore coordinate with  $x = 0$  at WG1 in Fig. 2.1; and  $n_p$  = porosity of the bottom sediment ( $n_p = 0.4$  in this experiment). Eq. (1) is integrated from arbitrary  $x$  to the landward boundary location  $x_m$  of  $q_x = 0$  (no overwash) where  $x_m = 19.9$  m in Fig. 2.5. The resultant equation is integrated from time  $t_1$  to subsequent time  $t_2$  to obtain the time-averaged rate  $\overline{q_x}$

$$\overline{q_x}(x) = \frac{1-n_p}{t_2-t_1} \int_x^{x_m} [Z_b(t_2, x) - Z_b(t_1, x)] dx \quad (2)$$

The measured elevations  $Z_b(x)$  at time  $t_1$  and  $t_2$  are used to estimate the average rate  $\overline{q_x}$  during the time interval  $(t_2-t_1)$ .

Fig. 2.5 shows the cross-shore variations of  $\overline{q_x}$  for the interval of E0-E10 and E10-E20 with  $(t_2-t_1) = 4,000$ s. The true equilibrium profile requires  $Z_b(t_2, x) = Z_b(t_1, x)$  and  $\overline{q_x} = 0$ . The absolute value of  $\overline{q_x}$  may be used to estimate the degree of deviation from the true equilibrium profile. The deviation decreased from E0-E10 to E10-E20 as

expected from the concept of equilibration under constant forcing. The error or uncertainty of the cross-shore sand transport  $\overline{q_x}$  in this experiment is of the order of  $0.002 \text{ cm}^2/\text{s}$  ( $8 \text{ cm}^2/4,000\text{s}$ ).

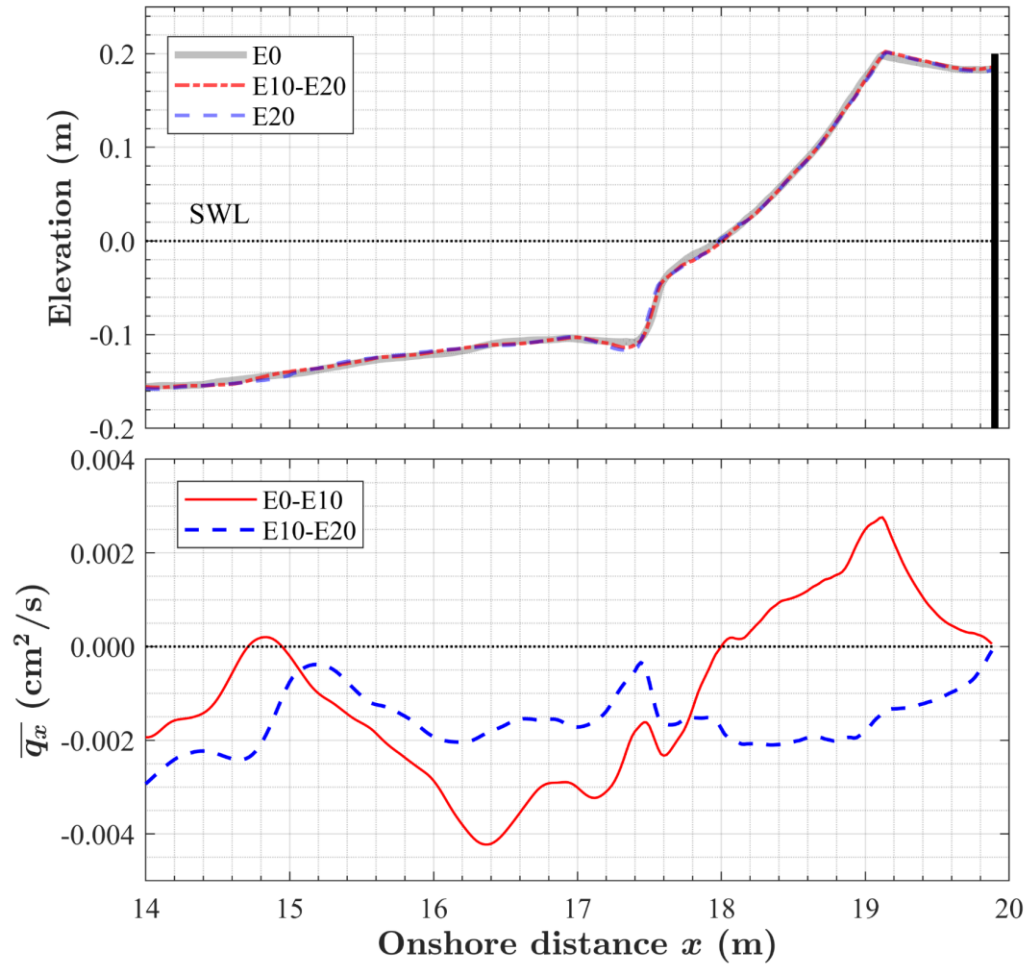


Figure 2.5 Measured profiles E0, E10, and E20 and cross-shore sand transport rate  $\overline{q_x}$  during the intervals of E0-E10 and E10-E20.

The measured profiles S0, S10, and S20 in the S test are shown in Fig. 2.6. The initial steep profile S0 was eroded rapidly and approached equilibrium in view of the similarity between the profiles S10 and S20. The sand transport rate  $\bar{q}_x$  calculated using Eq. (2) for S0-S10 is negative and offshore. The maximum offshore transport rate exceeds  $0.06 \text{ cm}^2/\text{s}$  in the vicinity of the still water shoreline at  $x = 18 \text{ m}$ . The calculated  $\bar{q}_x$  for S10-S20 is of the order of  $0.005 \text{ cm}^2/\text{s}$  and larger than the error estimate of  $0.002 \text{ cm}^2/\text{s}$ . The S test was terminated in anticipation of gradual approach to equilibrium.

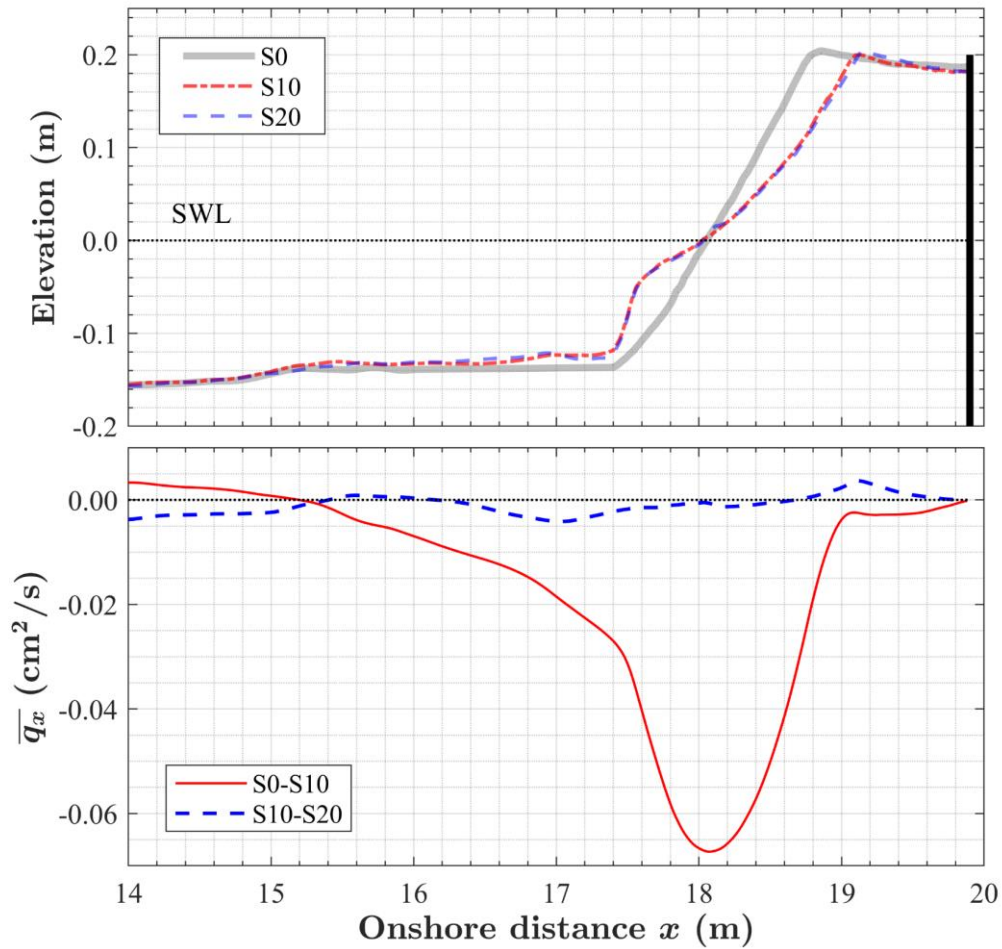


Figure 2.6 Measured profiles S0, S10, and S20 and cross-shore sand transport rate  $\bar{q}_x$  during the intervals of S0-S10 and S10-S20.

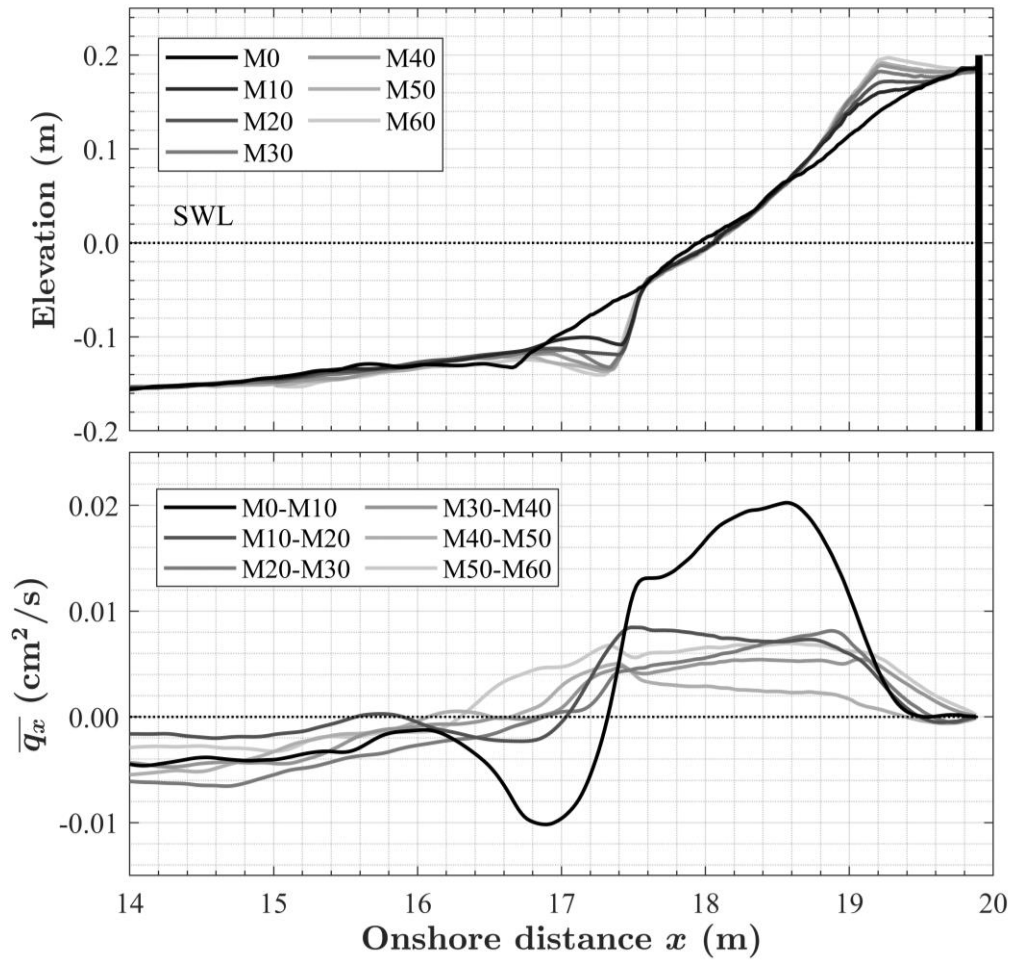


Figure 2.7 Measured profiles M0, M10, M20, M30, M40, M50, and M60 and cross-shore sand transport rate  $\overline{q_x}$  during the six intervals from M0-M10 to M50-M60.

Fig. 2.7 shows the measured seven profiles and the time-averaged sand transport rates during the six intervals in the M test. Onshore sand transport on the mild slope resulted in gradual berm growth in the upper swash zone. The toe at  $x = 17$  m of the mild foreshore of M0 was eroded rapidly to create a step in the lower swash zone. The transformation of the mild foreshore to the equilibrium foreshore in the E test is rapid

for erosion under breaking waves but slow for accretion under wave runup. The onshore sand transport rate  $\overline{q_x}$  for M0-M10 increases to 0.02 cm<sup>2</sup>/s and decreases to zero at the vertical wall ( $x = 19.9$  m). For the subsequent intervals (M10-M20 to M50-M60), the onshore sand transport rates remains of the order of 0.005 cm<sup>2</sup>/s for the gradual berm buildup on the initial mild foreshore.

## Chapter 3

### ANALYTICAL MODEL

The simple analytical model of Kobayashi et al. (2018) is applied to elucidate the foreshore slope effect on the cross-shore sediment transport rate  $q_x$ . Kobayashi et al. (2008) proposed bed load and suspended load formulas used in the cross-shore numerical model CSHORE (Kobayashi 2016). The formulas were simplified to derive the equilibrium profile popularized by Dean (1991). The simplification included the assumptions of shallow water, negligible wave setup, depth-limited breaking wave height, and still water depth  $h$  decreasing monotonically landward. The simplified formula for  $q_x$  is expressed as

$$q_x = \alpha h^{1.5} + \beta h^{1.5} \frac{\partial h^{1.5}}{\partial x} \quad \text{for } h > 0 \quad (3)$$

where  $h$  = still water depth;  $\alpha$  ( $\text{m}^{0.5}/\text{s}$ ) = bed load factor; and  $\beta$  ( $\text{s}^{-1}$ ) = suspended load factor. For the equilibrium profile with  $q_x = 0$ , Eq. (3) yields the equilibrium profile (Dean 1991)

$$h = A(x_0 - x)^{2/3}; A = \left(\frac{\alpha}{\beta}\right)^{2/3} \quad \text{for } q_x = 0 \quad (4)$$

where  $A$  = profile scale factor ( $\text{m}^{1/3}$ ); and  $x_0$  = cross-shore location of  $h = 0$ .

The analytical model based on Eqs. (3) and (4) is applied to estimate  $q_x(x)$  on the specified beach profile  $Z_b(x)$  and sediment parameter  $A$ . The still water depth  $h(x)$  and bottom slope  $S_b(x)$  are given by

$$h = -Z_b; \quad S_b = \frac{dZ_b}{dx} > 0 \quad (5)$$

where the bottom elevation is assumed to increase monotonically landward. Eq. (3) is rewritten as

$$q_x = \alpha h^{1.5} \left(1 - \frac{S_b}{S_e}\right); \quad S_e = \frac{2A^{1.5}}{3\sqrt{h}} \quad (6)$$

where  $S_e$  = equilibrium bottom slope because  $q_x = 0$  for  $S_b = S_e$ . For  $S_b > S_e$ ,  $q_x$  is negative and offshore. For  $S_b < S_e$ ,  $q_x$  is positive and onshore. The initial profiles of the three tests in Fig. 2.3 were decided in view of Eq. (6).

For actual applications, Eq. (6) is adjusted to compensate its shortcomings. The calculated  $q_x$  becomes sensitive to irregular slope fluctuations in the nearshore zone of small  $S_b$  and  $S_e$ . The upper bound  $h_t$  of the still water depth  $h$  is introduced in the following calculations. The depth  $h_t$  may be regarded as the toe depth of a relatively steep foreshore landward of a gentle nearshore slope. Moreover, Eq. (6) predicts  $q_x = 0$  for  $h = 0$  in contradiction to the measured  $\bar{q}_x$  in Figs. 2.6 and 2.7. Eq. (6) is adjusted by replacing  $h^{1.5}$  by  $h_t^{1.5}$  and setting the upper limit  $S_s$  of the calculated  $S_e$  near and above the SWL shoreline. The limiting slope  $S_s$  is taken as the slope in the swash zone of the equilibrium profile. The adjusted model is expressed as

$$q_x = \alpha h_t^{1.5} \left(1 - \frac{S_b}{S_e}\right) \quad \text{for } h \leq h_t \quad (7)$$

where use is made of  $q_x = 0$  for  $h > h_t$  to indicate the seaward limit of the model applicability. The equilibrium slope is estimated as

$$S_e = \frac{2A^{1.5}}{3\sqrt{h}} \leq S_s \quad \text{for } h > 0 \quad (8)$$

where  $S_e = S_s$  for  $h \leq 0$  and  $Z_b \geq 0$ . The input parameters of the simple model are the toe depth  $h_t$ , profile scale factor  $A$ , swash slope  $S_s$ , and load factor  $\alpha$ . The value of  $\alpha$  determines the order of magnitude of  $q_x$ .

## Chapter 4

### LABORATORY DATA COMPARISON

The measured equilibrium profile of E10 and the sand transport rate during E10-E20 are used to estimate the model input parameters. Fig. 4.1 compares the measured and fitted profiles for E10 where  $h_t = 0.11$  m,  $A = 0.1$  m<sup>1/3</sup>, and  $S_s = 0.2$ . The measured profile E10 does not satisfy the monotonic increase of the bottom elevation in the vicinity of the foreshore toe. As a result, the fitting procedure is somewhat arbitrary. The parameter  $A$  for the sand diameter  $d_{50} = 0.18$  mm is estimated using the formula in Dean and Darymple (2002). The equilibrium profile of Eq. (4) is fitted to the measured profile for the zone of  $0 < h < h_t = 0.11$  m. The bottom slope in the seaward zone of  $h > h_t$  is approximately 0.013 and too small to apply Eq. (7) which is too sensitive to the small  $S_e$  of the order of 0.01 or less. The shoreline location of  $x_0$  in Eq. (4) is not used in the analytical model based on Eq. (7) and (8) because  $S_e$  depends on the depth  $h$  below the SWL instead of the offshore distance ( $x_0 - x$ ) from the shoreline. The swash slope  $S_s$  in Fig. 4.1 increases upward but  $S_s = 0.2$  is adopted to represent the upper swash slope where the sand transport rate approaches zero. Available swash slope data were analyzed by Kriebel et al. (1991) and Creed et al. (2000) but the data variability was too large to estimate  $S_s$  accurately.

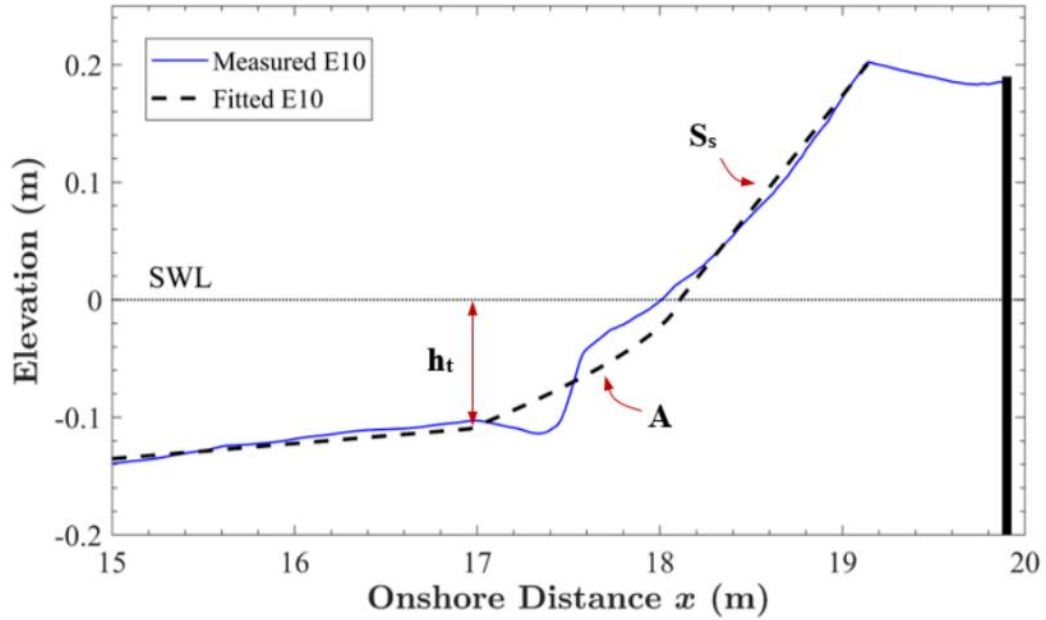


Figure 4.1 Analytical equilibrium profile model fitted to measured equilibrium profile E10 where the toe depth  $h_t$ , profile scale factor  $A$ , and swash slope  $S_s$  are input to the model.

The measured rate  $\bar{q}_x$  of the order of  $0.002 \text{ cm}^2/\text{s}$  for E10-E20 in Fig. 2.5 is compared in Fig. 4.2 with the analytical rate  $q_x$  given by Eqs. (7) and (8) for the measured profiles  $Z_b(x)$  of E10 and E20 where Eq. (5) is used to calculate  $h(x)$  and  $S_b(x)$  for each profile. The load factor  $\alpha$  in Eq. (7) is taken as  $10^{-4} \text{ (m}^{1/2}/\text{s)}$  for the subsequent comparison with the S and M tests. The computed  $q_x$  for the E test is too large even though  $q_x$  is computed only in the zone of  $h < h_t$  on the steep step and foreshore. The analytical model based on the slopes  $S_b$  and  $S_e$  is sensitive to the disagreement between the measured and fitted equilibrium profiles. It is noted that  $\alpha = 10^{-5} \text{ (m}^{1/2}/\text{s)}$  was used

for the initial calibration for the E test to predict the measured order of magnitude of  $\overline{q_x}$ .

However,  $\alpha = 10^{-4}$  (m<sup>1/2</sup>/s) is necessary for the S and M tests.

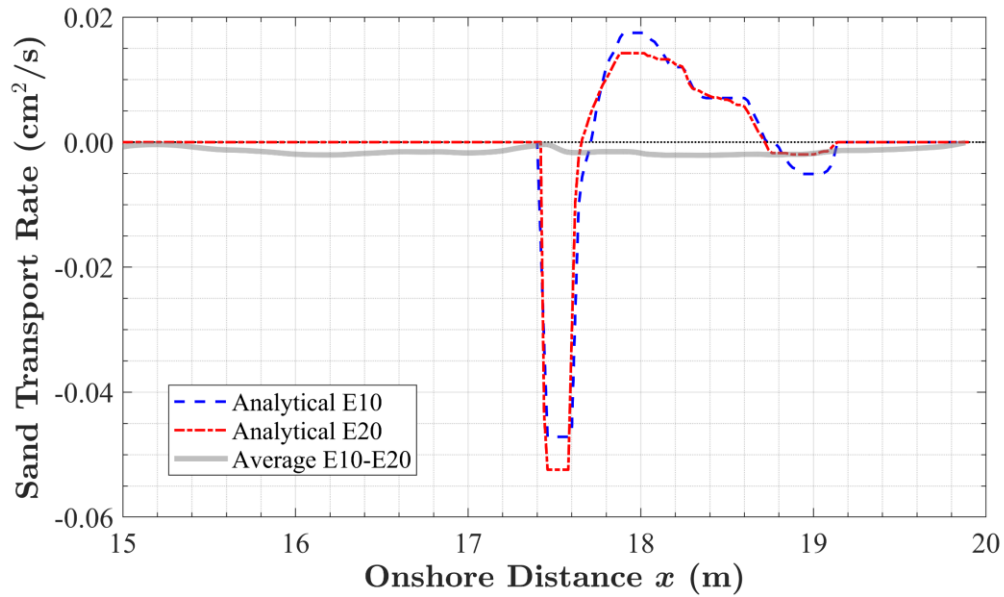


Figure 4.2 Analytical sand transport rate  $q_x$  predicted for each of the measured profiles of E10 and E20 in comparison to average rate  $\overline{q_x}$  during the interval of E10-E20.

Fig. 4.3 compares the analytical rates  $q_x$  for S0 and S10 with the average rate  $\overline{q_x}$  for S0-S10 in Fig. 2.6. The analytical  $q_x$  for S0 predicts the offshore sand transport on the initial step foreshore but cannot produce the offshore sand transport on the gentle slope seaward of the foreshore toe. The agreement deteriorates for S10 after the formation of the step (Fig. 2.6). The analytical  $q_x$  for S20 is very similar to that of S10 because of the similarity of the measured profiles S10 and S20. Fig. 4.4 compares the analytical rates  $q_x$  for M0 and M10 with the averaged rate  $\overline{q_x}$  for M0-M10 in Fig. 2.7. The analytical  $q_x$  for M0 predicts the onshore sand transport on the initial mild

foreshore. The analytical  $q_x$  for M10 predicts onshore sand transport on the foreshore but produces unrealistic rates in the scour zone seaward of the foreshore toe. The cross-shore variations of the analytical  $q_x$  for M20, M30, M40, M50, and M60 are similar to that of M10 and omitted for brevity.

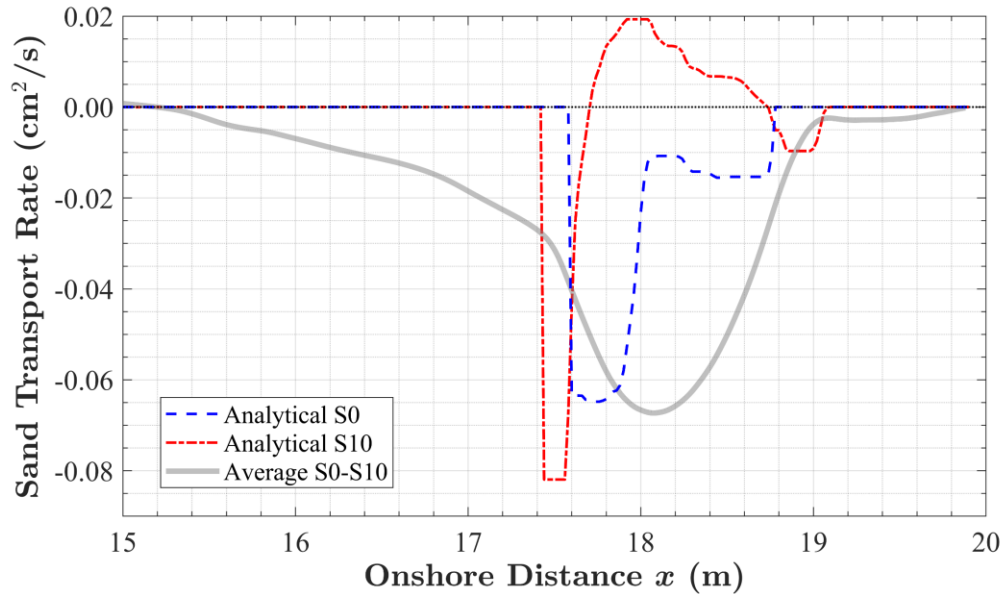


Figure 4.3 Analytical sand transport rate  $q_x$  predicted for each of the measured profiles of S0 and S10 in comparison to average rate  $\overline{q_x}$  during the interval of S0-S10.

The equilibrium profile in this specific experiment is not represented well by the equilibrium profile in the form of Eq. (4). Additional experiments should be conducted for different sediments and wave conditions in order to evaluate the generality of the proposed simple analytical model. The utility of the model is the estimation of cross-shore sediment transport in the absence of wave data. In the following, the model is

applied to the beach nourishment project of Pattaya in Thailand presented by Laksanalamai and Kobayashi (2021 and 2022).

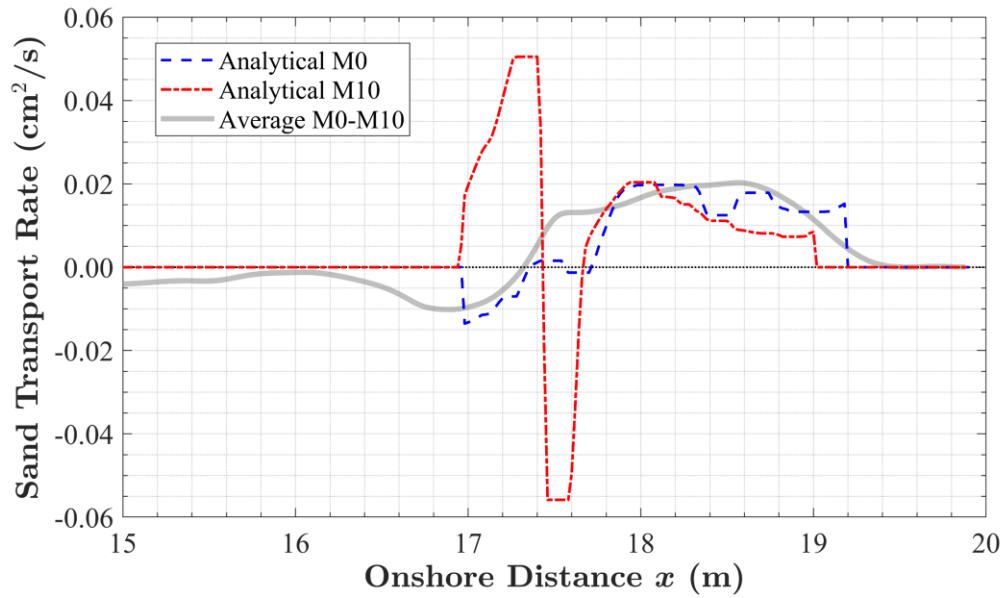


Figure 4.4 Analytical sand transport rate  $q_x$  predicted for each of the measured profiles of M0 and M10 in comparison to average rate  $\overline{q_x}$  during the interval of M0-M10.

## Chapter 5

### **PATTAYA BEACH**

Pattaya beach is located in the northern Gulf of Thailand which is a square area with an opening on its southern side only, as shown in Fig. 5.1. The length of the square area is about 100 km and the average water depth is 15 m. The Pattaya beach is microtidal with the average tidal range of 1.5 m. The average significant wave height is 0.2 m and the wave energy is low. Pattaya is a famous resort near Bangkok but its beach almost disappeared. The beach was widened by placing 363,000 m<sup>3</sup> of medium sand ( $d_{50} = 0.35$  mm) along the shoreline length of 2.8 km between two terminal groins constructed in 2018. The bathymetry and topography were measured in 2015 before the first major beach nourishment in Thailand and in 2019, 2020, 2021, 2022, and 2023 after the sand placement. The water level and waves were not measured for this annual monitoring program with limited funding. The analytical model is applied to assist the interpretation of the survey data.

Satellite images of Pattaya beach have been available since 2005 (Google Earth Pro, TerraMetrics and Maxar Technologies). The dry beach width was very narrow even in 2005. Fig. 5.2 shows a satellite image on 22 October 2022. Fig. 5.3 shows that the nourished wide beach remained after 4 years of the sand placement between the south (lower leftward in Fig. 5.2) and north groins of 60 m length. The predominant wave direction is from the south through the southern opening of the northern Gulf of

Thailand. The north groin was constructed normal to the rocky shore to reduce the northward longshore sand transport where a rocky beach is located north of the nourished beach. Waves from the south are diffracted around the cape south of Pattaya. The diffracted waves cause southward sand transport in the sheltered zone where a harbor was constructed. The south groin was constructed to reduce local southward longshore sand transport.



Figure 5.1 Pattaya beach location in Thailand (ArcGIS Pro).

The bathymetry and topography data are analyzed to estimate the sand volume changes during 2015-2023 and the beach profile changes along 30 cross-shore lines (L1-L30) in Fig. 5.4. All the cross-shore lines are represented by three points at the onshore distance of  $x = 0$  m, 600 m, and 710 m. The curved line at  $x = 710$  m corresponds to the vertical wall with its crest elevation of 3 m above the mean sea level. The curved line of



Figure 5.2 Pattaya beach (Google earth Pro) on October 22, 2022 after the sand placement ( $130 \text{ m}^3/\text{m}$ ) between the south and north groins constructed in 2018.

$x = 600 \text{ m}$  is the seaward boundary of the nourished sand placement. The water depth along the curved line of  $x = 0$  is in the range of 4-5 m. The maximum significant wave height during severe storms was estimated to be about 2 m using wind data during 1981-2009 and limited wave data during 10 months in 1997 as explained by Laksanalamai and Kobayashi (2021) who analyzed the survey data of 2015, 2019, and 2020. The seaward boundary  $x = 0$  may be located outside the surf zone during severe storms.

Sand volume changes in the seaward ( $x = 0\text{-}600 \text{ m}$ ) and landward ( $x = 600\text{-}710 \text{ m}$ ) segments between the south (L1-L20) and north (L20-L30) sections are calculated and presented in Table 5.1. The north section is regarded to be affected by the north groin. The sand placement in the landward segment before the 2019 survey increased the sand volume by 257K ( $1\text{K} = 1,000 \text{ m}^3$ ) and 105K in the south and north sections, respectively.



(a) After sand placement (February 2019)



(b) After one year (February 2020)



(c) North terminal groin (February 2020)



(d) North terminal groin (January 2021)



(e) After two years (January 2021)



(f) South terminal groin (January 2021)



(g) South terminal groin (March 2023)



(h) North terminal groin (March 2023)



(i) After four years (March 2023)



(j) After four years (March 2023)



(k) North terminal groin (March 2023)



(l) After four years (March 2023)

Figure 5.3 Pattaya beach during 2019-2023 after sand placement.

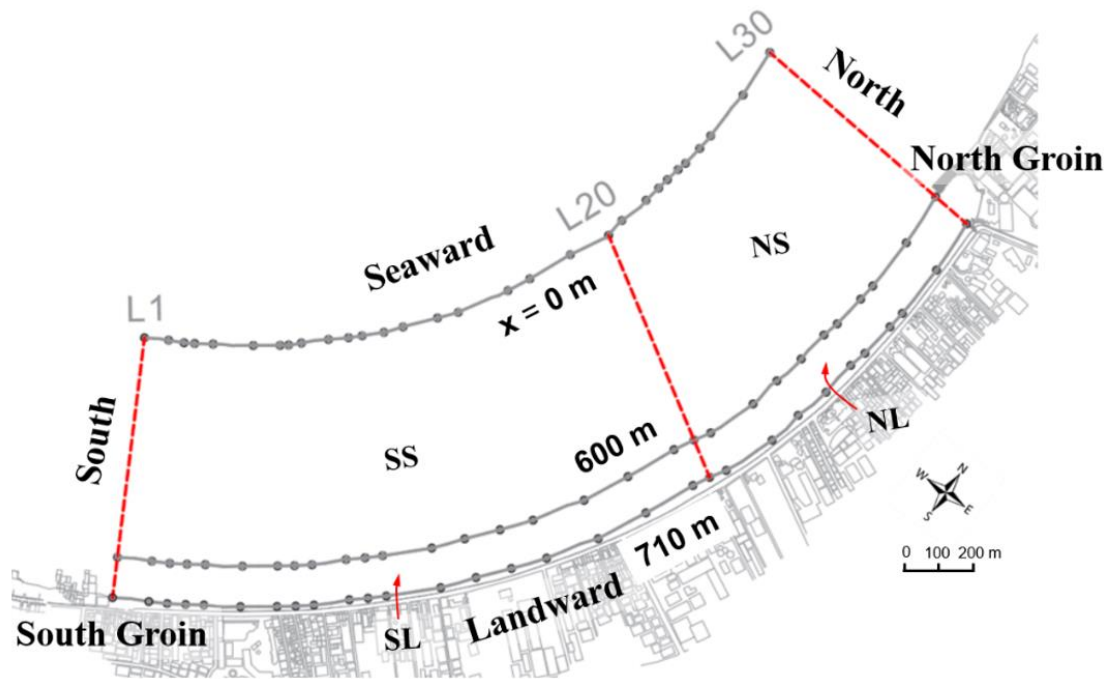


Figure 5.4 Thirty cross-shore lines (L1-L30) and four zones (SL, SS, NL, and NS) for the sand volume changes during 2015-2023.

The sum of 362K is practically the same as the nourished sand volume of 363K. The sand volume in both sections decreased during 2019-2020 and increased slightly during the three intervals during 2020-2023. As for the seaward segment, the large volume changes in the south and north sections during 2015-2019 and 2019-2020 appeared to be correlated as analyzed by Laksanalamai and Kobayashi (2021) but the causes of the large volume changes were uncertain. The smaller volume changes during the three intervals during 2020-2023 may indicate stabilization from disturbances created by the nourishment project. The sand volumes during 2015-2023 in Table 5.1 increased in the SL, SS, and NL zones and decreased noticeably in the NS zone in Fig. 5.4. The increase of the sand volume in the SL and NL zones was not expected for Pattaya beach which

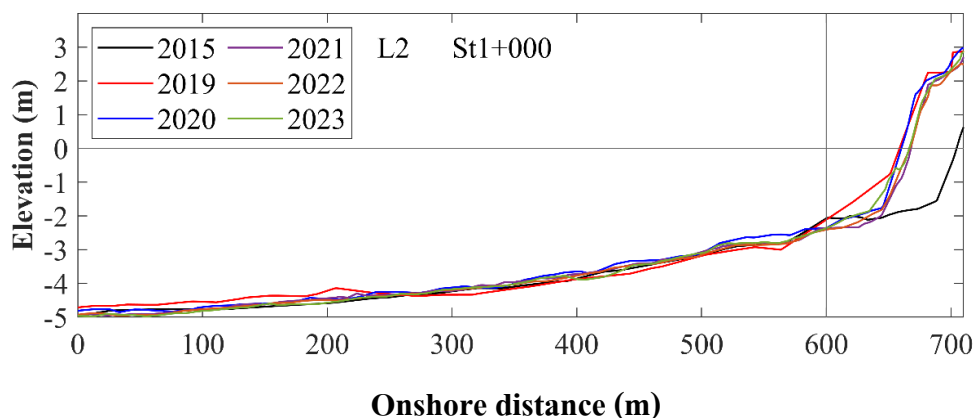
was suffering chronic erosion before the beach nourishment project. Houston (2023) examined the fate of sand placed over a 20-year period at Panama City, Florida where the wave climate is relatively benign, except of hurricanes. About 87% of the placed sand remained on profiles. Low wave energy at Pattaya beach may have contributed to the apparent stability of the nourished beach during 2019-2023.

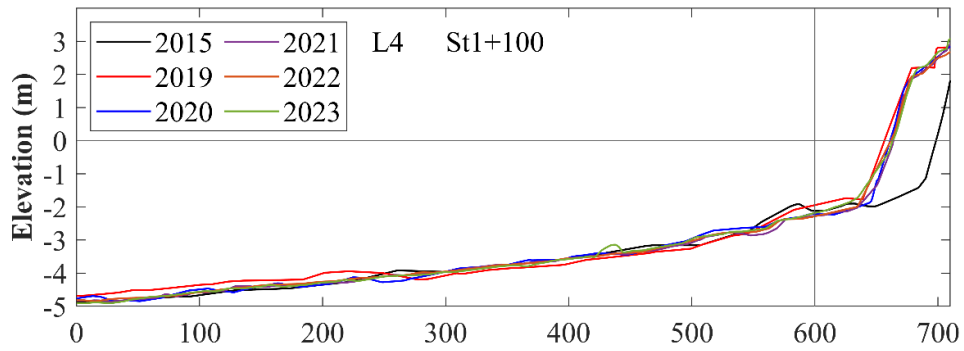
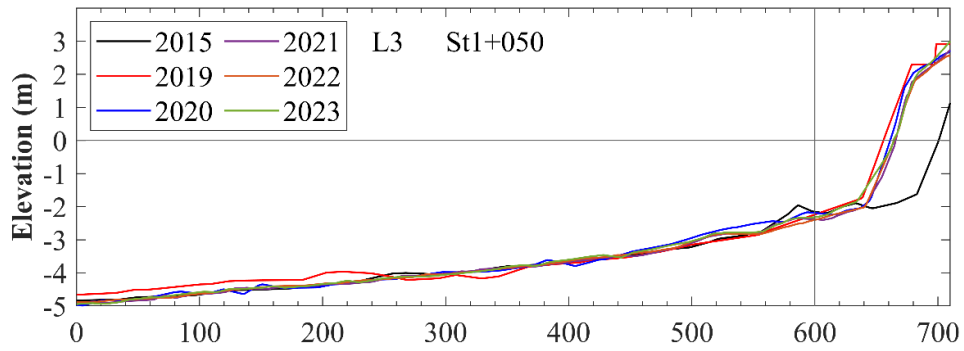
**Table 5.1.** Sand volume changes (1K = 1,000 m<sup>3</sup>) in four zones in the South (S) and North (N) segments separated into the Landward (L) and Seaward (S) sections.

Interval	Landward Zone		Seaward Zone	
	South	North	South	North
2015-2019	257K	105K	50K	-139K
2019-2020	-27K	-22K	54K	-107K
2020-2021	1K	26K	-13K	10K
2021-2022	17K	0K	-17K	10K
2022-2023	25K	16K	-39K	-4K
<b>2015-2023</b>	<b>273K</b>	<b>125K</b>	<b>35K</b>	<b>-230K</b>

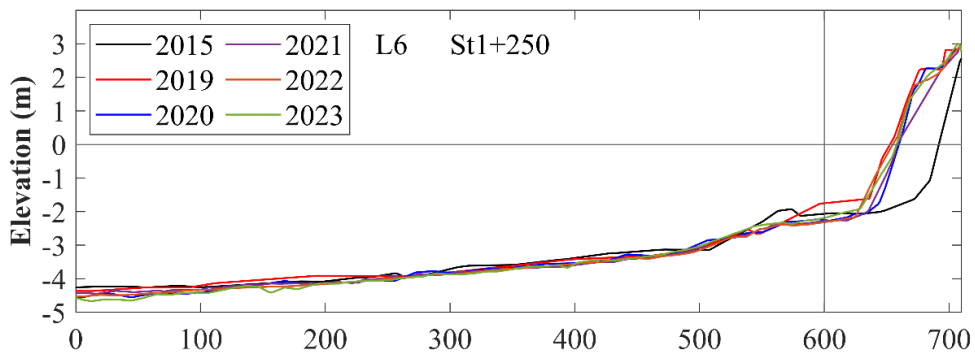
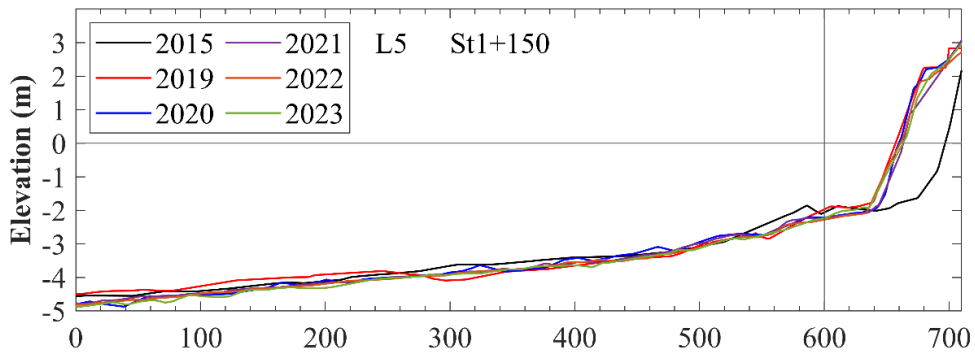
The survey was conducted in January (2015), February (2019, 2020, and 2021), or March (2022 and 2023).

The measured profile changes along L1-L30 are analyzed to infer sediment transport patterns. Line L1 is excluded from the following data analysis since no sand was placed along L1 because of expected sand accretion north of the south groin. The measured six profiles along each line are plotted together in Fig. 5.5 to examine the temporal variations. The 19 (10) profiles of L2-L20 (L21-L30) in each year are plotted together to inspect the alongshore variability because the beach slope is gentler in the north section in Fig. 5.5. Figs. 5.6 and 5.7 show the alongshore averaged profiles in the south and north sections in 2015, 2019, 2020, 2021, 2022, and 2023, respectively. The landward segment ( $x = 600-710$  m) is stretched laterally to distinguish the six lines in Figs. 5.6 and 5.7. The beach profiles in the SS zone in Fig. 5.6 did not change much during 2015-2023 and the corresponding sand volume changes were relatively small in Table 5.1. The bottom elevation lowering during 2015-2019 and 2019-2020 in the NS zone in Fig. 5.7 explains the large sand volume loss in the NS zone in Table 5.1. The nourished sand placed on the 2015 profile remained mostly in the SL and NL zones in Figs. 5.6 and 5.7. This is consistent with the relatively small sand volume changes during 2019-2023 in the landward segment in Table 5.1.

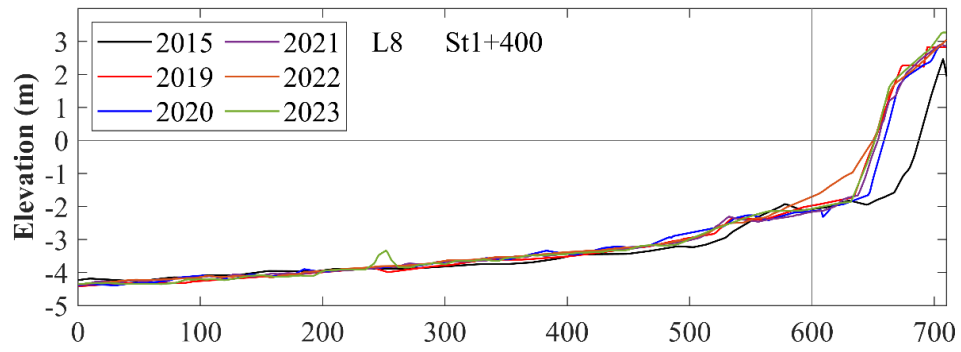
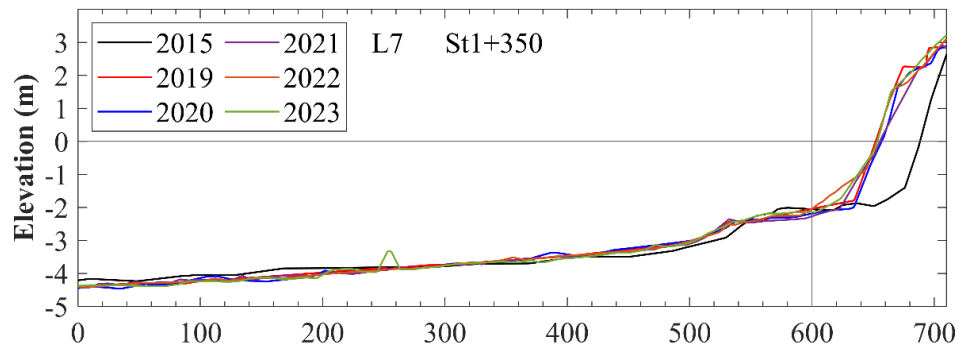




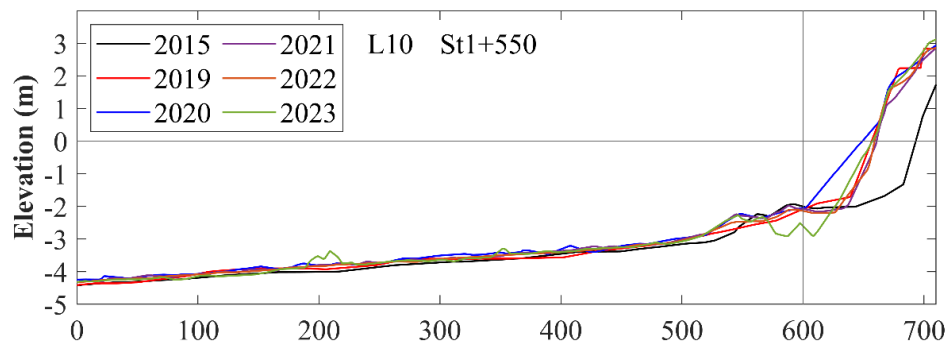
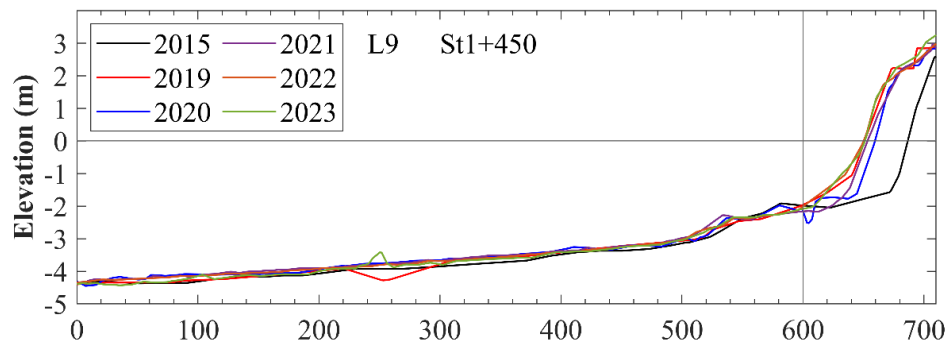
Onshore distance (m)



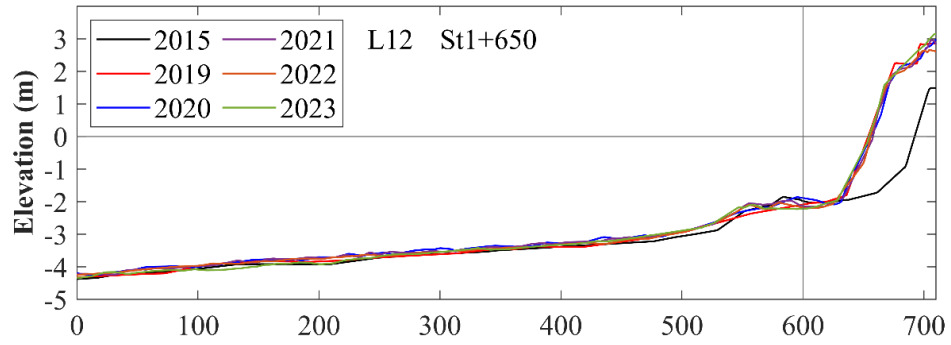
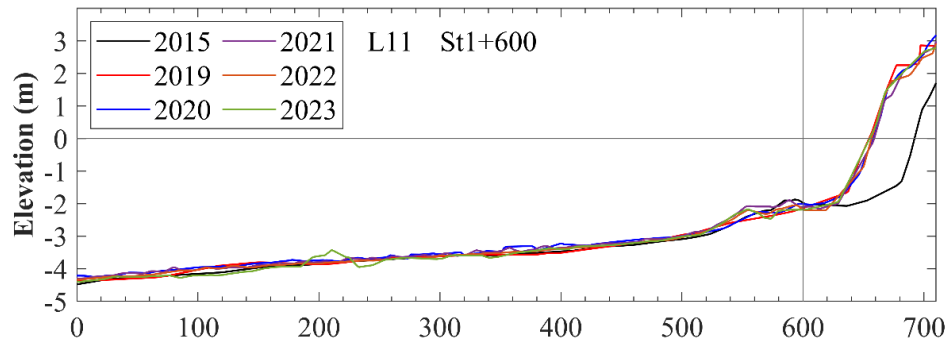
Onshore distance (m)



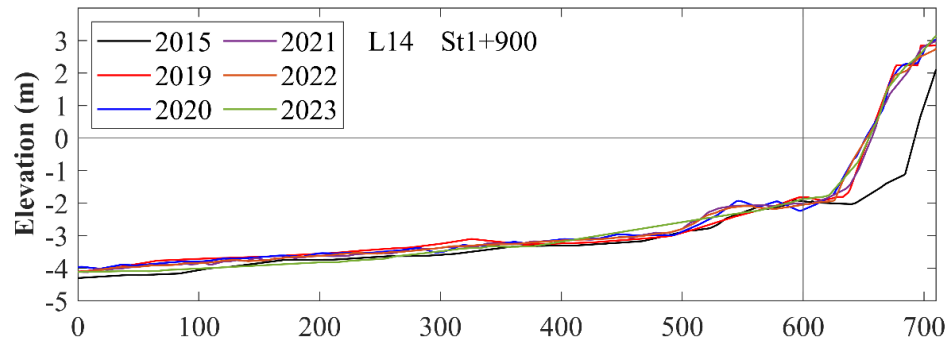
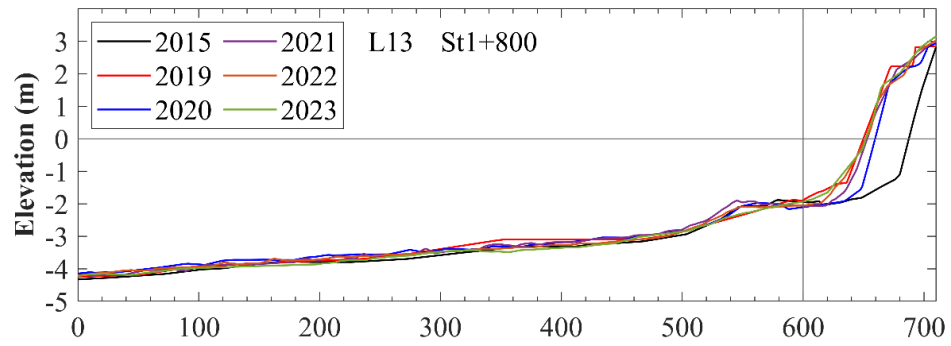
**Onshore distance (m)**



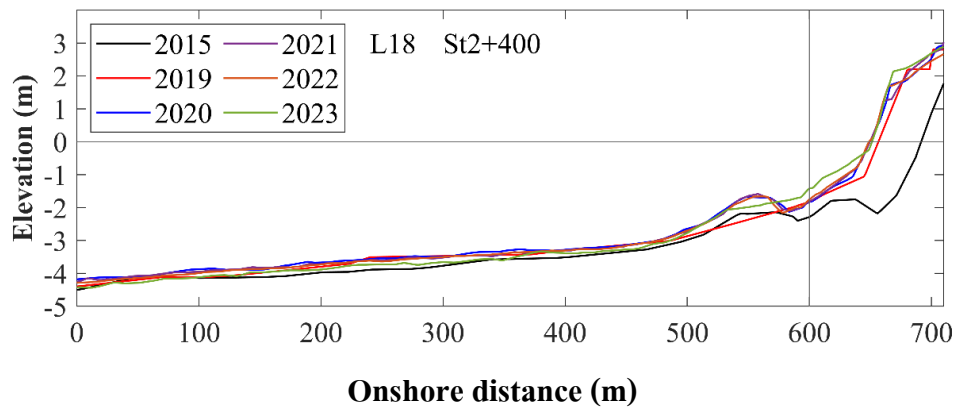
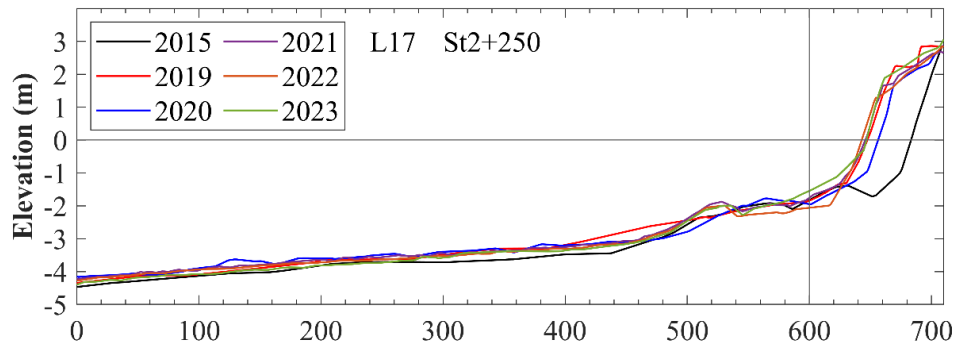
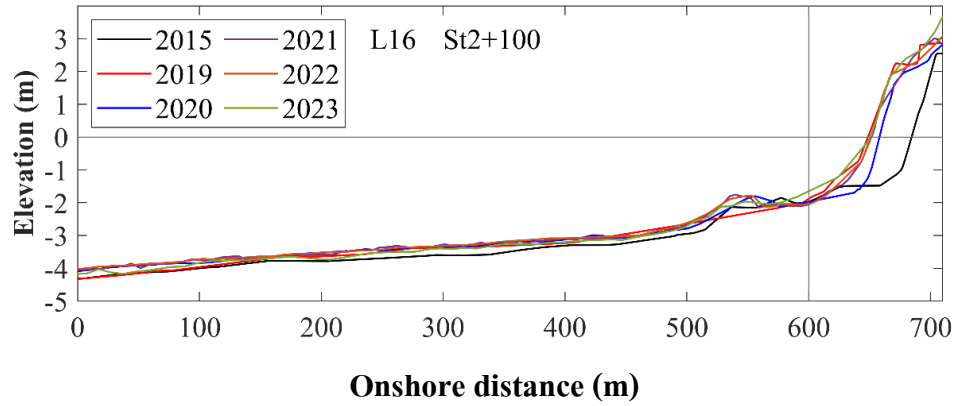
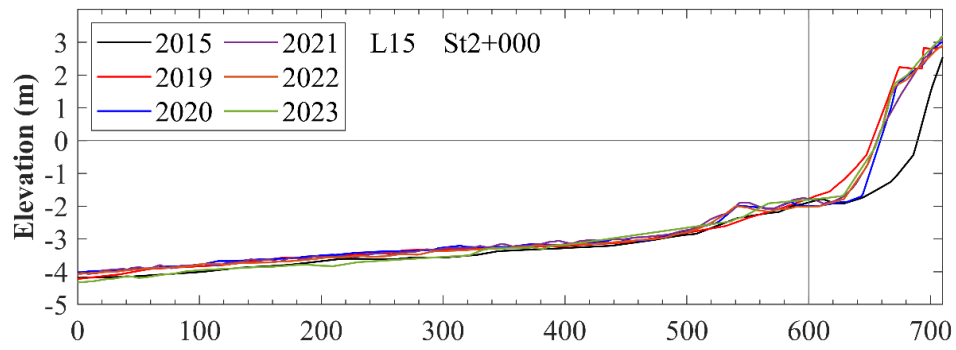
**Onshore distance (m)**

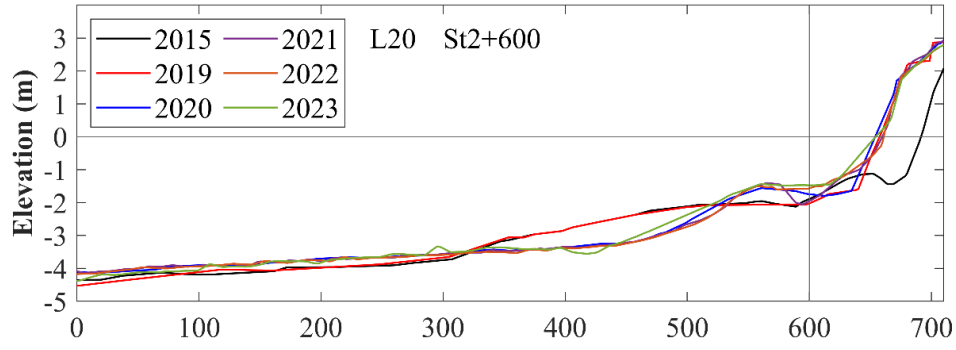
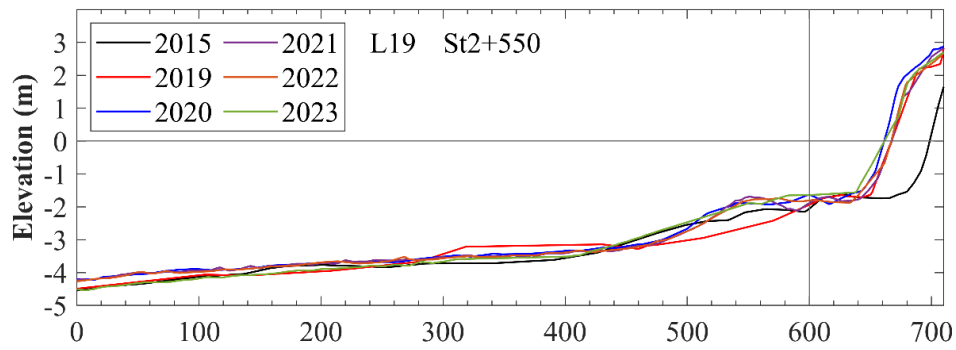


**Onshore distance (m)**

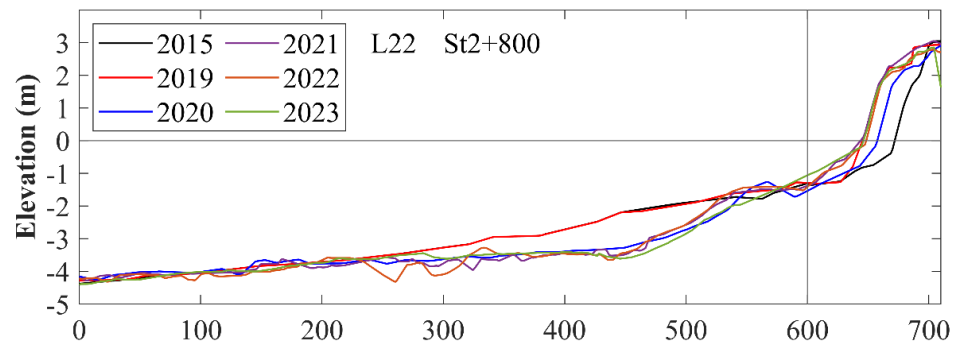
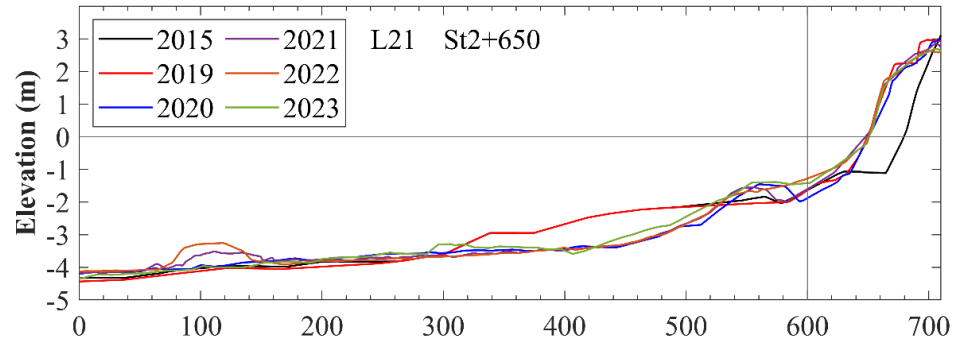


**Onshore distance (m)**

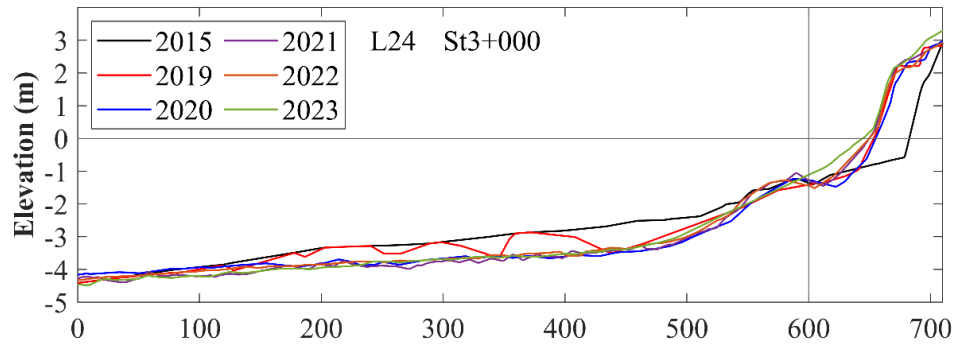
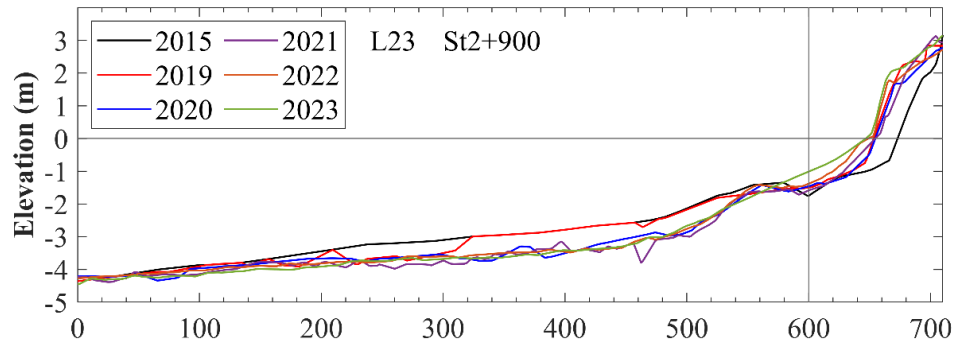




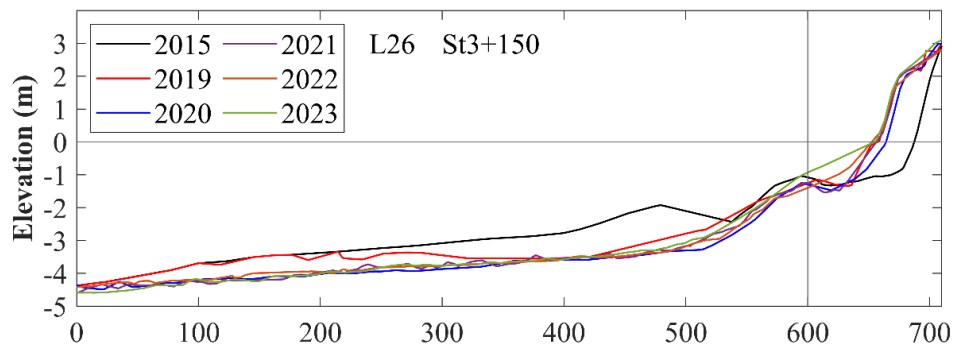
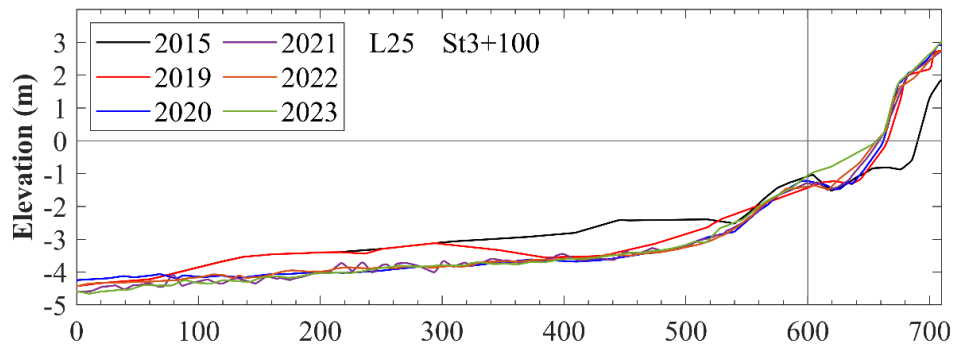
**Onshore distance (m)**



**Onshore distance (m)**



**Onshore distance (m)**



**Onshore distance (m)**

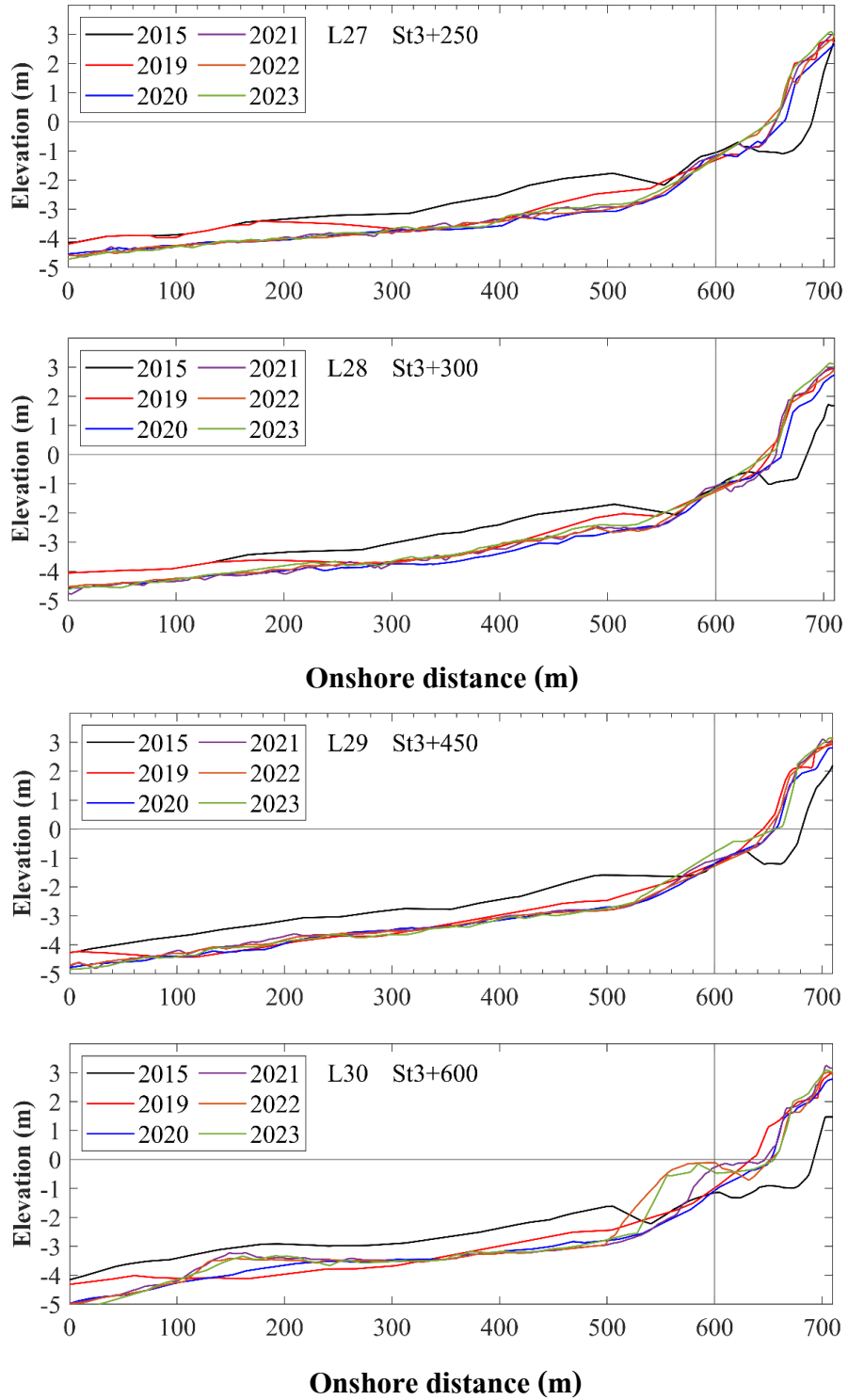


Figure 5.5 Measured profile changes (L2-L30) in 2015, 2019, 2020, 2021, 2022, and 2023.

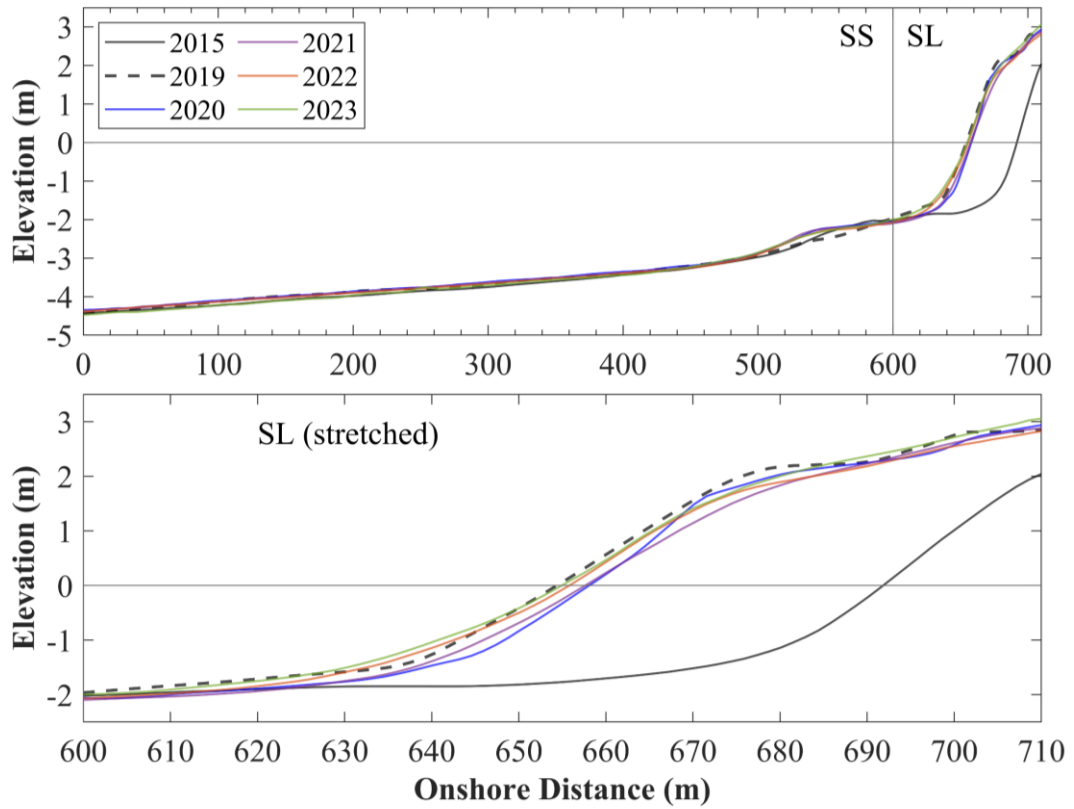


Figure 5.6. Alongshore averaged profiles in the south zones of SS and SL in 2015, 2019, 2020, 2021, 2022, and 2023.

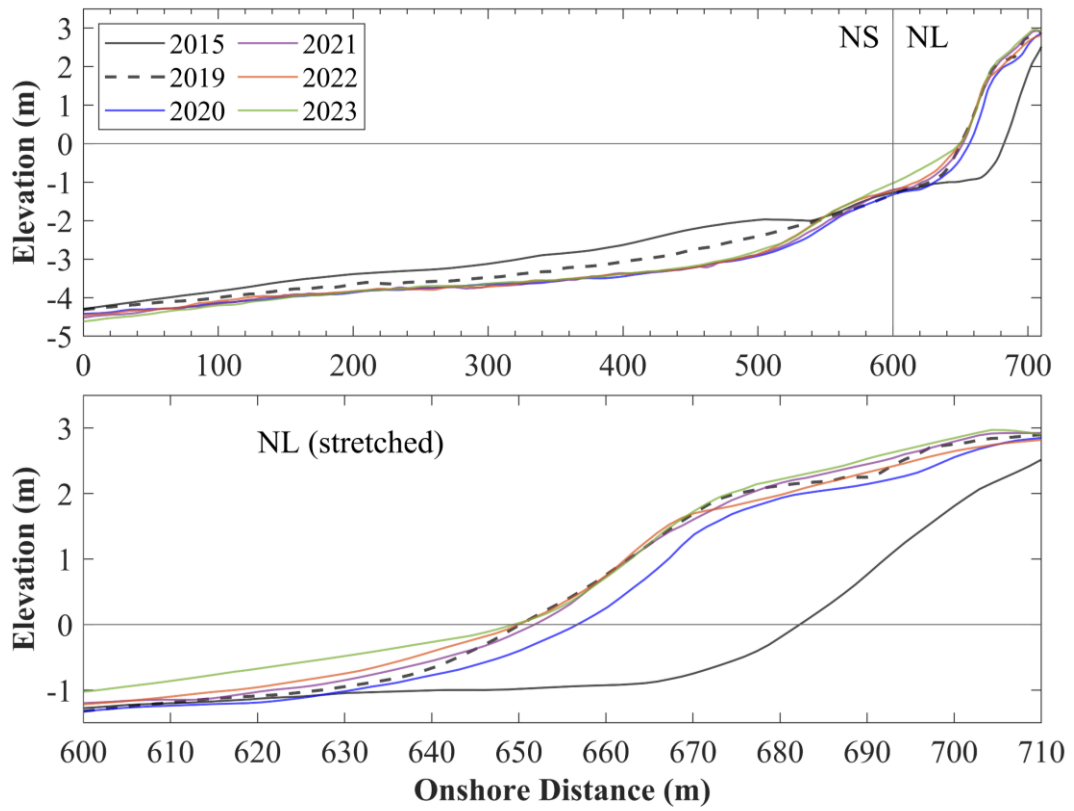


Figure 5.7 Alongshore averaged profiles in the north zones of NS and NL in 2015, 2019, 2020, 2021, 2022, and 2023.

## Chapter 6

### FIELD DATA COMPARISON

The alongshore averaged profiles are used to estimate the cross-shore sand transport rates based on Eq. (2) where  $x_m = 710$  m at the vertical wall of no wave overtopping. For the laboratory data,  $Z_b(x)$  in Eq. (2) is the alongshore averaged profile in the wave flume of 1.15-m width and the assumption of alongshore uniformity in Eq. (1) is appropriate. For the field data in Fig. 5.4, the assumption of alongshore uniformity needs to be scrutinized. The interval  $(t_2-t_1)$  in Eq. (2) corresponds to the four intervals during 2019-2023 in Table 5.1 and  $(t_2-t_1)$  is 12 or 13 months. Fig. 6.1 shows the average cross-shore sand transport rate  $\overline{q_x}$  estimated using Eq. (2) for the SS and SL zones in Fig. 5.6. The offshore (negative) sand transport rate during 2019-2020 is the maximum near  $x = 600$  m at the toe of the nourished foreshore. The location of the maximum offshore rate is shifted offshore during 2020-2021. The rate  $\overline{q_x}$  is shifted upward and becomes positive (onshore) during 2021-2022. The onshore sand transport rate is the maximum at  $x = 440$  m during 2022-2023. The estimated values of  $\overline{q_x}$  are of the order of  $10 \text{ m}^2/\text{y}$  ( $0.003 \text{ cm}^2/\text{s}$ ) which is the same order of magnitude as  $0.002 \text{ (cm}^2/\text{s)}$  in Fig. 2.5 for the laboratory E test. However, constant waves were used in the laboratory experiment, whereas waves and water level vary in time at Pattaya beach. Van Rijn (1997) estimated the onshore sediment transport rate of  $5\text{-}10 \text{ m}^2/\text{y}$  in 20-m depth in

Holland, Dean and Houston (2016) estimated the onshore rate of  $3 \text{ m}^2/\text{y}$  along the southwestern coast of Florida. Kobayashi and Jung (2012) computed beach erosion and recovery using the cross-shore model CSHORE (Kobayashi 2016) and obtained the computed onshore rate of about  $20 \text{ m}^2/\text{y}$  in 9-m depth in Delaware. The rates  $\bar{q}_x$  in Fig. 6.1 based on the assumption of alongshore uniformity may not be accurate but may not be unreasonable either.

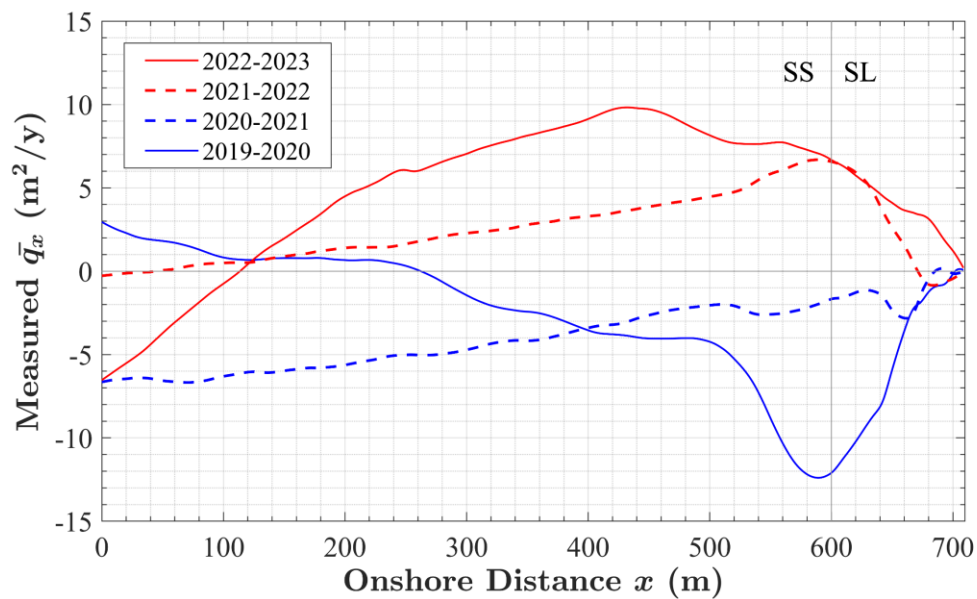


Figure 6.1 Annual cross-shore sand transport rate  $\bar{q}_x$  for the four intervals (2019-2023) estimated using alongshore averaged profiles in the south zones (SS and SL) and assuming alongshore uniformity.

Fig. 6.2 shows the average rates  $\bar{q}_x$  estimated for the NS and NL zones in Fig. 5.7. The offshore rate  $\bar{q}_x$  during 2019-2020 increased offshore and reached  $100 \text{ m}^2/\text{y}$  (not shown in Fig. 6.2) at  $x = 0$  because of conspicuous erosion in the NS zone during 2019-2020. This erosion must have been caused mostly by alongshore sediment loss as

explained in relation to Table 5.1. The rates  $\bar{q}_x$  for the other three intervals during 2020-2023 are positive (onshore) and of the order of 10-20 m<sup>2</sup>/y. Some of the sand lost alongshore during 2019-2020 might have returned during 2020-2023. The sediment transport processes in the north section are more complicated probably because of the proximity to the north groin.

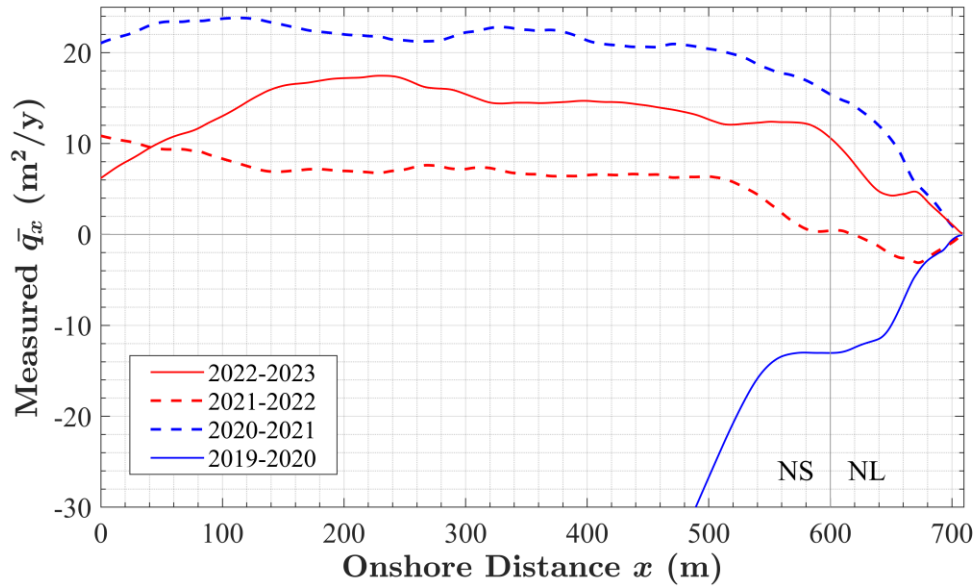


Figure 6.2 Annual cross-shore sand transport rate  $\bar{q}_x$  for the four intervals (2019-2023) estimated using alongshore averaged profiles in the north zones (NS and NL).

The analytical model based on Eqs. (7) and (8) is compared with the measured rates  $\bar{q}_x$  in Figs. 6.1 and 6.2. For the south section, the rate  $\bar{q}_x$  in the SL zone is close to zero for the interval 2020-2021. The average profile of the measured profiles of 2020 and 2021 is used to obtain the fitted values of  $h_t = 2.0$  m,  $A = 0.14$  m<sup>1/3</sup>, and  $S_s = 0.098$  as listed in Table 6.1 which includes the fitted values for the laboratory beach in Fig. 4.1. For the sand with  $d_{50} = 0.35$  mm,  $A = 0.14$  m<sup>1/3</sup> is consistent with the formula in

Dean and Dalrymple (2002). The fitted profile is compared with the average profile of the 2020 and 2021 profiles in the top panel of Fig. 6.3. The beach slope in the seaward zone of  $h > h_t$  is 0.003. The landward limit of the comparison is taken at  $x = 680$  m between the foreshore and berm. The average rate  $\overline{q_x}$  in Fig. 6.1 is compared with the average analytical rate of  $q_x$  computed at the beginning and end year of each interval. Fig. 6.3 shows the comparisons for the intervals of 2019-2020 and 2022-2023 corresponding to the minimum  $\overline{q_x}$  and the maximum  $\overline{q_x}$  in the SL zone in Fig. 6.1. The load factor  $\alpha$  is chosen as  $10^{-7}$  m<sup>1/2</sup>/s to predict the measured order of magnitude for the average rate  $\overline{q_x}$ . The average analytical  $q_x$  fluctuates between positive (onshore) and negative (offshore) values because the fitted profile does not represent the bottom slope of the assumed equilibrium profile sufficiently.

Table 6.1 Equilibrium foreshore slope model parameters for the laboratory beach and Pattaya beach.

Parameter	Laboratory beach	Pattaya beach	
		South	North
Median diameter $d_{50}$ (mm)	0.18	0.35	0.35
Scale factor $A$ (m <sup>1/3</sup> )	0.10	0.14	0.09
Toe depth $h_t$ (m)	0.11	2.0	1.9
Swash slope $S_s$	0.20	0.098	0.086
Load factor $\alpha$ (m <sup>1/2</sup> /s)	$10^{-4}$	$10^{-7}$	$10^{-7}$

For the north section, the average  $\overline{q_x}$  for 2021-2022 is close to zero in Fig. 6.2. The average of the measured profiles of 2021 and 2022 (Fig. 5.7) is used to obtain  $h_t = 1.9$  m,  $A = 0.09$  m<sup>1/3</sup> and  $S_s = 0.086$ . Table 6.1 compares the fitted values in the north and south sections. The typical value of  $A = 0.14$  m<sup>1/3</sup> for  $d_{50} = 0.35$  mm is reduced to  $A = 0.09$  m<sup>1/3</sup> in the north section influenced by the north groin. The average profile of 2021 and 2022 and the fitted profile are compared in the top panel in Fig. 6.4. The agreement for the north section is better than that of the laboratory beach (Fig. 4.1) and that for the south section (Fig. 6.3). The average  $\overline{q_x}$  (negative) during 2019-2020 is compared with the average analytical  $q_x$  for 2019 and 2020 in the middle panel. The average  $\overline{q_x}$  (positive) during 2022-2023 is compared with the average analytical  $q_x$  for 2022 and 2023. The analytical  $q_x$  fluctuates in the range of (-5)-5 m<sup>2</sup>/y unlike the average  $\overline{q_x}$  based on the measured profile change in Eq. (2). This discrepancy suggests that the measured profile change is partly caused by alongshore sand loss (2019-2020) or gain (2022-2023), which is neglected in the analytical model.

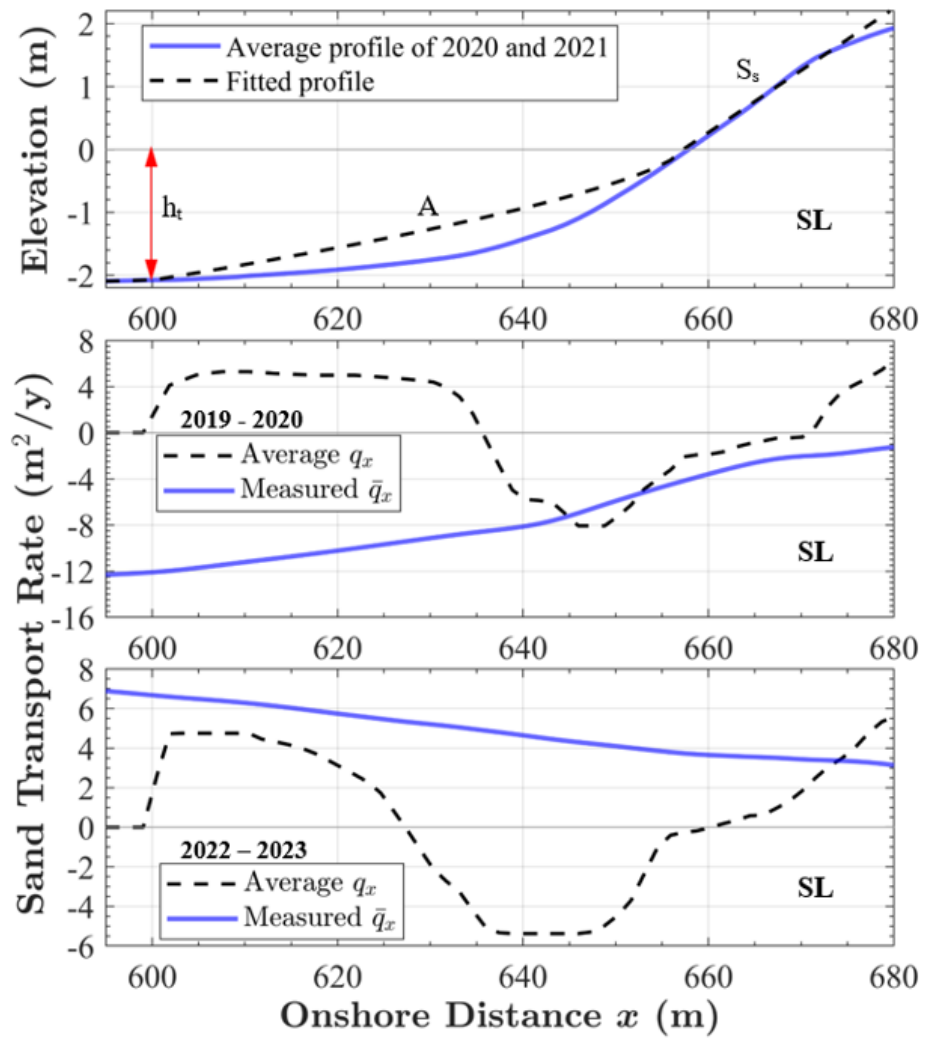


Figure 6.3 Estimation of model parameters  $h_t$ ,  $A$ , and  $S_s$  for the SL zone, and comparison of measured sand transport rate  $\bar{q}_x$  and average analytical rate  $q_x$  during 2019-2020 and 2022-2023.

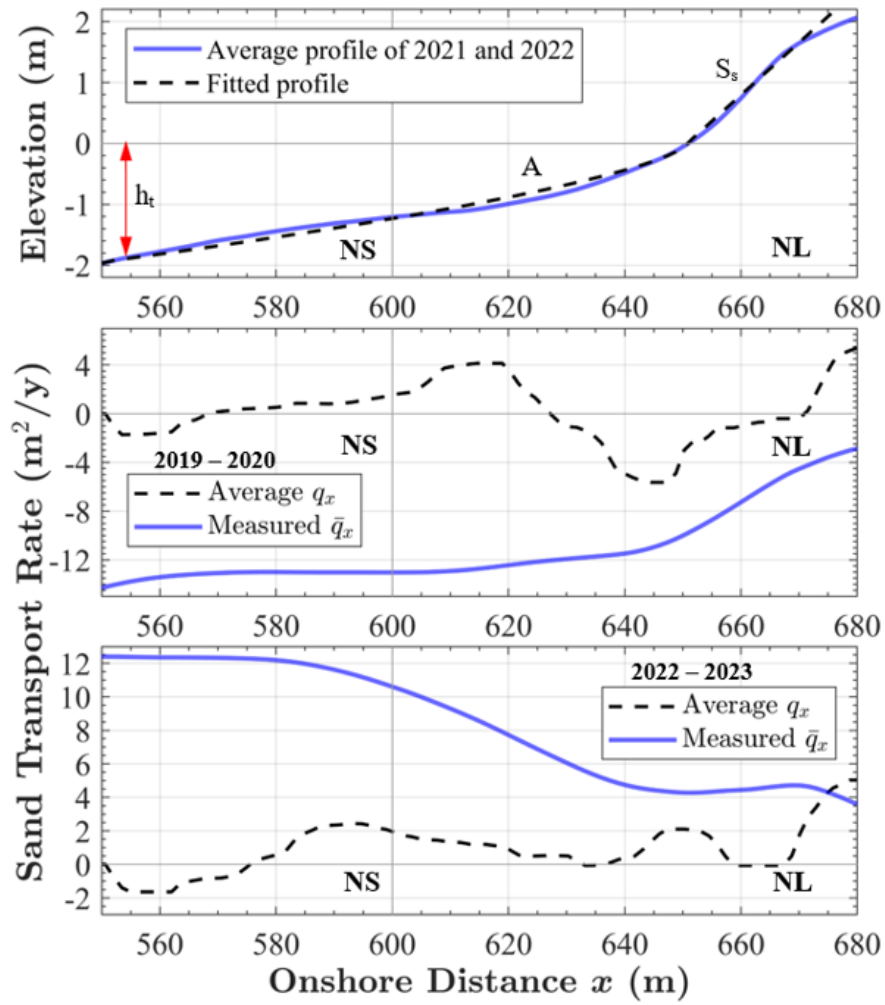


Figure 6.4 Estimation of  $h_t$ ,  $A$ , and  $S_s$  for the NL and NS zone, and comparison of measured sand transport rate  $\bar{q}_x$  and average analytical rate  $q_x$  during 2019-2020 and 2022-2023.

## Chapter 7

### **CONCLUSIONS**

This study introduces a simple analytical model proposed to estimate cross-shore sediment transport on a measured beach profile in the absence of wave data. The model predicts offshore (onshore) sediment transport on the foreshore slope which is steeper (milder) than the equilibrium foreshore slope. The equilibrium slope diminishes as still water depth increases and sediment diameter decreases. The sediment transport rate is influenced by the ratio of the measured beach slope and the equilibrium slope. An experiment was conducted in a wave flume to evaluate and adjust the simple model. Equilibrium, steep, and mild foreshores were created on a beach consisting of fine sand and exposed to irregular waves with the offshore significant wave height of 0.2 m. The steep foreshore experienced rapid erosion and became equilibrium. The mild foreshore underwent swift transformation near its toe in the lower swash zone due to wave uprush and downrush collision. Berm growth, on the other hand, on the mild slope in the upper swash zone was gradual, indicating slow recovery. The cross-shore sediment transport rates on the initially steep and mild foreshores were predicted reasonably when the foreshore profiles exhibited clear deviations from the assumed equilibrium profile which differed from the measured equilibrium profile with a steep step in the lower swash zone.

The adjusted analytical model is tested using data from the nourished beach at Pattaya, Thailand. The beach was widened by placing  $130 \text{ m}^3/\text{m}$  of medium sand along the shoreline length of 2.8 km stretch between two terminal groins in 2018. The significant wave height is 0.2 m on the average but may increase to 2 m during severe storms. During 2019-2023, the bathymetry and topography were measured yearly but water level and waves were not measured due to limited funding. The surveyed data were analyzed to estimate sand volume changes and beach profile changes. The sand volume and beach profile in the area of the sand placement were surprisingly stable during 2019-2023. The analytical model based on the assumption of alongshore uniformity is applied to interpret the estimated cross-shore sediment transport rate per unit width of the order of  $10 \text{ m}^2/\text{y}$ . The analytical model can be useful for field data with significant beach slope changes. In a related study, Zhu and Kobayashi (2023) used the numerical model CSHORE (Kobayashi 2016) to predict the recovery of an eroded and flattened beach in front of a rubble mound structure during 2015 and 2020. The dry beach width increased more than 80 m in front of the structure. This recovery is consistent with the analytical model which predicts onshore sand transport on the flattened and mild slope as demonstrated in this laboratory experiment.

## REFERENCES

- Creed, C.G., Bodge, K.R., and C.L. Suter. 2000. "Construction slopes for beach nourishment projects." *J. Waterway, Port, Coastal, Ocean Eng.* 126(1): 57-62.
- Dalrymple, R.A. 1992. "Prediction of storm/ normal beach profiles." *J. Waterway, Port, Coastal, Ocean Eng.* 118(2): 193-200.
- Dean, R.G. 1991. "Equilibrium beach profiles: Characteristics and applications." *J. Coastal Res.* 7(1): 53-84.
- Dean, R.G. and R.A. Dalrymple. 2002. *Coastal processes with engineering applications.* United Kingdom: Cambridge University Press.
- Dean, R.G., and J.R. Houston. 2016. "Determining shoreline response to sea level rise." *Coastal Eng.* 114(Aug): 1-8.
- Goda, Y. 2010. *Random seas and design of maritime structures.* Singapore: World Scientific.
- Houston, J.R. 2023. "Measured fate of beach nourishment sand." *J. Coastal Res.* 39(3): 407-417.
- Kobayashi, N. 1987. "Analytical solution for dune erosion by storms." *J. Waterway, Port, Coastal, Ocean Eng.* 113(4): 401-418.
- Kobayashi, N. 2016. "Coastal sediment transport modeling for engineering applications." *J. Waterway, Port, Coastal, Ocean Eng.* 142(6): 03116001.

- Kobayashi, N. and H. Jung. 2012. "Beach erosion and recovery." *J. Waterway, Port, Coastal, Ocean Eng.* 138(6): 473-483.
- Kobayashi, N., Payo, A., and L. Schmied. 2008. "Cross-shore suspended sand and bed load transport on beaches." *J. Geophys. Res.* 113(C7): C07001.
- Kobayashi, N., Zhu, T., and S. Mallavarapu. 2018. "Equilibrium beach profile with net cross-shore sand transport." *J. Waterway, Port, Coastal, Ocean Eng.* 144(6): 04018016.
- Kriebel, D.L., and R.G. Dean (1985). "Numerical simulation of time-dependent beach and dune erosion." *Coastal Eng.* 9: 221-245.
- Kriebel, D.L., Kraus, N.C., and M. Larson. 1991. "Engineering methods for predicting beach profile response." In *Proc., Coastal Sediments 1991 Specialty Conf. Quantitative Approaches to Coastal Sediment Processes*, 557-571. New York: ASCE.
- Laksanalamai, J. and N. Kobayashi. 2021. "Evolution of a nourished sand beach under low wave energy in Thailand." *Shore & Beach* 89(3): 36-40.
- Laksanalamai, J. and N. Kobayashi. 2022. "Performance of a nourished sand beach in the upper Gulf of Thailand." *J. Coastal and Offshore Science and Engineering.* 2(2022): 46-55.
- Laksanalamai, J., and N. Kobayashi. 2023. "Tracking of small discrete objects submerged in surf and swash zones on sand beaches." *J. Waterway, Port, Coastal, Ocean Eng.* 149(6): 04023017.

USACE (US Army Corps of Engineers) 2003. Coastal engineering manual.

Washington, DC: USACE.

Van Rijn, L.C. (1997). "Sediment transport and budget of the central zone of Holland." Coastal Eng. 32(1): 61-90.

Zhu, T. and N. Kobayashi. 2023. "Recovery of eroded beach seaward of closed Katrina cut in Dauphin Island, Alabama." J. Coastal Offshore Science Eng. 2(1): 1-12.

**APPENDIX**  
**A HYDRODYNAMIC DATA FOR EQUILIBRIUM, STEEP, AND MILD**  
**SLOPE TESTS**

Table A.1 Incident wave characteristics, Test E1-E20

<b>Run</b>	$H_{mo}$ (cm)	$H_{rms}$ (cm)	$H_s$ (cm)	$T_p$ (s)	$T_s$ (s)	$R$
<b>E1</b>	19.76	13.97	19.22	2.62	2.16	0.163
<b>E2</b>	20.32	14.37	19.81	2.62	2.17	0.164
<b>E3</b>	20.45	14.46	19.77	2.62	2.15	0.159
<b>E4</b>	20.49	14.49	19.82	2.62	2.15	0.159
<b>E5</b>	20.46	14.47	19.82	2.62	2.14	0.156
<b>E6</b>	20.49	14.49	19.84	2.62	2.14	0.158
<b>E7</b>	20.48	14.48	19.74	2.62	2.12	0.156
<b>E8</b>	20.47	14.48	19.76	2.62	2.13	0.161
<b>E9</b>	20.48	14.48	19.91	2.62	2.18	0.160
<b>E10</b>	20.43	14.45	19.72	2.62	2.15	0.155
<b>E11</b>	19.78	13.99	19.08	2.62	2.14	0.158
<b>E12</b>	20.42	14.44	19.79	2.62	2.16	0.162
<b>E13</b>	20.65	14.60	19.96	2.62	2.13	0.162
<b>E14</b>	20.68	14.62	19.88	2.62	2.13	0.157
<b>E15</b>	20.68	14.62	19.89	2.62	2.16	0.157
<b>E16</b>	20.70	14.63	19.96	2.62	2.17	0.158
<b>E17</b>	20.66	14.61	19.91	2.62	2.13	0.160
<b>E18</b>	20.68	14.62	19.95	2.62	2.14	0.157
<b>E19</b>	20.64	14.60	19.86	2.62	2.14	0.157
<b>E20</b>	20.67	14.62	20.00	2.62	2.15	0.156
<b>Average</b>	20.47	14.47	19.78	2.62	2.15	0.159

Table A.2 Incident wave characteristics, Test S1-S20

<b>Run</b>	<b><math>H_{mo}</math> (cm)</b>	<b><math>H_{rms}</math> (cm)</b>	<b><math>H_s</math> (cm)</b>	<b><math>T_p</math> (s)</b>	<b><math>T_s</math> (s)</b>	<b><math>R</math></b>
<b>S1</b>	20.06	14.18	19.31	2.62	2.15	0.187
<b>S2</b>	20.45	14.46	19.77	2.62	2.16	0.174
<b>S3</b>	20.50	14.50	19.80	2.62	2.15	0.176
<b>S4</b>	20.53	14.51	19.78	2.62	2.16	0.174
<b>S5</b>	20.50	14.50	19.78	2.62	2.15	0.171
<b>S6</b>	20.45	14.46	19.58	2.62	2.14	0.169
<b>S7</b>	20.50	14.50	19.87	2.62	2.17	0.168
<b>S8</b>	20.43	14.45	19.71	2.62	2.17	0.167
<b>S9</b>	20.48	14.48	19.86	2.62	2.17	0.170
<b>S10</b>	20.45	14.46	19.80	2.62	2.17	0.164
<b>S11</b>	20.00	14.14	19.40	2.62	2.16	0.174
<b>S12</b>	20.29	14.35	19.58	2.62	2.14	0.167
<b>S13</b>	20.38	14.41	19.65	2.62	2.15	0.167
<b>S14</b>	20.45	14.46	19.85	2.62	2.16	0.169
<b>S15</b>	20.41	14.43	19.73	2.62	2.14	0.166
<b>S16</b>	20.44	14.45	19.68	2.62	2.16	0.169
<b>S17</b>	20.39	14.42	19.70	2.62	2.13	0.163
<b>S18</b>	20.38	14.41	19.64	2.62	2.14	0.167
<b>S19</b>	20.39	14.41	19.62	2.62	2.14	0.165
<b>S20</b>	20.35	14.39	19.61	2.62	2.15	0.166
<b>Average</b>	20.39	14.42	19.69	2.62	2.15	0.170

Table A.3 Incident wave characteristics, Test M1-M60

<b>Run</b>	$H_{mo}$ (cm)	$H_{rms}$ (cm)	$H_s$ (cm)	$T_p$ (s)	$T_s$ (s)	$R$
<b>M1</b>	19.92	14.09	19.08	2.62	2.15	0.146
<b>M2</b>	20.35	14.39	19.73	2.62	2.16	0.145
<b>M3</b>	20.38	14.41	19.57	2.62	2.13	0.149
<b>M4</b>	20.38	14.41	19.59	2.62	2.11	0.151
<b>M5</b>	20.40	14.43	19.73	2.62	2.10	0.152
<b>M6</b>	20.40	14.43	19.60	2.62	2.11	0.152
<b>M7</b>	20.38	14.41	19.80	2.62	2.14	0.158
<b>M8</b>	20.41	14.43	19.67	2.62	2.12	0.152
<b>M9</b>	20.40	14.43	19.61	2.62	2.11	0.153
<b>M10</b>	20.36	14.40	19.55	2.62	2.12	0.154
<b>M11</b>	20.11	14.22	19.48	2.62	2.15	0.156
<b>M12</b>	20.36	14.39	19.62	2.62	2.14	0.154
<b>M13</b>	20.45	14.46	19.65	2.62	2.13	0.159
<b>M14</b>	20.44	14.46	19.84	2.62	2.13	0.156
<b>M15</b>	20.42	14.44	19.64	2.62	2.13	0.155
<b>M16</b>	20.49	14.49	19.80	2.62	2.13	0.158
<b>M17</b>	20.44	14.45	19.87	2.62	2.13	0.154
<b>M18</b>	20.46	14.47	19.85	2.62	2.13	0.161
<b>M19</b>	20.44	14.46	19.67	2.62	2.14	0.159
<b>M20</b>	20.43	14.45	19.70	2.62	2.13	0.157
<b>M21</b>	19.72	13.94	19.07	2.62	2.16	0.157
<b>M22</b>	20.13	14.23	19.46	2.62	2.14	0.156
<b>M23</b>	20.15	14.25	19.59	2.62	2.15	0.164
<b>M24</b>	20.13	14.23	19.44	2.62	2.13	0.157
<b>M25</b>	20.14	14.24	19.49	2.62	2.15	0.157
<b>M26</b>	20.18	14.27	19.71	2.62	2.16	0.157
<b>M27</b>	20.20	14.28	19.66	2.62	2.16	0.156

<b>M28</b>	20.17	14.26	19.56	2.62	2.15	0.154
<b>M29</b>	20.20	14.28	19.53	2.62	2.13	0.159
<b>M30</b>	20.13	14.23	19.54	2.62	2.13	0.158
<b>M31</b>	19.83	14.02	19.27	2.62	2.14	0.155
<b>M32</b>	20.29	14.35	19.62	2.62	2.15	0.161
<b>M33</b>	20.45	14.46	19.76	2.62	2.15	0.164
<b>M34</b>	20.47	14.47	19.90	2.62	2.14	0.161
<b>M35</b>	20.46	14.46	19.77	2.62	2.14	0.163
<b>M36</b>	20.44	14.45	19.82	2.62	2.13	0.161
<b>M37</b>	20.43	14.45	19.80	2.62	2.14	0.158
<b>M38</b>	20.45	14.46	19.92	2.62	2.15	0.166
<b>M39</b>	20.40	14.42	19.71	2.62	2.14	0.159
<b>M40</b>	20.41	14.43	19.81	2.62	2.14	0.156
<b>M41</b>	19.82	14.01	19.24	2.62	2.14	0.164
<b>M42</b>	20.25	14.32	19.63	2.62	2.16	0.160
<b>M43</b>	20.29	14.35	19.80	2.62	2.16	0.158
<b>M44</b>	20.31	14.36	19.63	2.62	2.14	0.163
<b>M45</b>	20.33	14.37	19.64	2.62	2.15	0.162
<b>M46</b>	20.39	14.42	19.69	2.62	2.12	0.165
<b>M47</b>	20.33	14.37	19.60	2.62	2.14	0.160
<b>M48</b>	20.33	14.38	19.74	2.62	2.14	0.161
<b>M49</b>	20.32	14.37	19.69	2.62	2.14	0.158
<b>M50</b>	20.32	14.37	19.66	2.62	2.14	0.162
<b>M51</b>	19.77	13.98	19.28	2.62	2.17	0.165
<b>M52</b>	20.22	14.30	19.62	2.62	2.14	0.162
<b>M53</b>	20.25	14.32	19.73	2.62	2.16	0.157
<b>M54</b>	20.32	14.37	19.55	2.62	2.14	0.161
<b>M55</b>	20.32	14.37	19.73	2.62	2.16	0.164
<b>M56</b>	20.29	14.35	19.69	2.62	2.17	0.165
<b>M57</b>	20.25	14.32	19.71	2.62	2.15	0.161

<b>M58</b>	20.29	14.35	19.63	2.62	2.14	0.163
<b>M59</b>	20.23	14.30	19.62	2.62	2.18	0.158
<b>M60</b>	20.22	14.29	19.70	2.62	2.14	0.161
<b>Average</b>	20.28	14.34	19.63	2.62	2.14	0.158

Table A.4 Mean free-surface elevation  $\bar{\eta}$  (cm) at 8 wave gauge locations, Test E1-E20

<b>Run</b>	<b>WG1</b>	<b>WG2</b>	<b>WG3</b>	<b>WG4</b>	<b>WG5</b>	<b>WG6</b>	<b>WG7</b>	<b>WG8</b>
<b>E1</b>	-0.25	-0.26	-0.21	0.08	0.29	0.44	NR	10.52
<b>E2</b>	-0.23	-0.24	-0.15	0.14	0.35	0.50	NR	10.06
<b>E3</b>	-0.22	-0.21	-0.14	0.15	0.36	0.47	NR	10.07
<b>E4</b>	-0.20	-0.21	-0.19	0.16	0.36	0.49	NR	10.00
<b>E5</b>	-0.24	-0.23	-0.16	0.13	0.37	0.47	NR	10.04
<b>E6</b>	-0.20	-0.22	-0.16	0.16	0.38	0.45	NR	10.05
<b>E7</b>	-0.21	-0.21	-0.15	0.15	0.36	0.45	NR	9.98
<b>E8</b>	-0.24	-0.20	-0.16	0.16	0.37	0.51	NR	10.03
<b>E9</b>	-0.19	-0.20	-0.13	0.13	0.39	0.46	NR	9.99
<b>E10</b>	-0.22	-0.21	-0.17	0.16	0.37	0.45	NR	9.94
<b>E11</b>	-0.23	-0.21	-0.21	0.16	0.25	0.42	NR	10.58
<b>E12</b>	-0.20	-0.20	-0.16	0.20	0.36	0.46	NR	9.91
<b>E13</b>	-0.20	-0.27	-0.16	0.26	0.39	0.50	0.60	9.81
<b>E14</b>	-0.22	-0.21	-0.20	0.25	0.41	0.47	0.58	9.87
<b>E15</b>	-0.20	-0.21	-0.16	0.23	0.40	0.51	0.57	9.98
<b>E16</b>	-0.21	-0.21	-0.18	0.26	0.40	0.50	0.59	9.89
<b>E17</b>	-0.21	-0.21	-0.18	0.25	0.42	0.53	0.59	9.87
<b>E18</b>	-0.23	-0.19	-0.16	0.28	0.40	0.51	0.59	9.90
<b>E19</b>	-0.21	-0.21	-0.16	0.25	0.40	0.47	0.57	9.93
<b>E20</b>	-0.23	-0.19	-0.15	0.27	0.43	0.49	0.59	9.87
<b>Average</b>	-0.22	-0.22	-0.17	0.19	0.37	0.48	0.59	10.01

NR implies “not reliable” data

Table A.5 Mean free-surface elevation  $\bar{\eta}$  (cm) at 8 wave gauge locations, Test S1-S20

<b>Run</b>	<b>WG1</b>	<b>WG2</b>	<b>WG3</b>	<b>WG4</b>	<b>WG5</b>	<b>WG6</b>	<b>WG7</b>	<b>WG8</b>
<b>S1</b>	-0.20	-0.19	-0.20	0.23	0.38	0.50	0.58	NR
<b>S2</b>	-0.23	-0.22	-0.17	0.30	0.42	0.48	0.47	14.77
<b>S3</b>	-0.24	-0.24	-0.21	0.29	0.43	0.50	0.53	14.06
<b>S4</b>	-0.22	-0.21	-0.20	0.29	0.44	0.51	0.54	13.45
<b>S5</b>	-0.19	-0.21	-0.16	0.30	0.44	0.53	0.52	12.89
<b>S6</b>	-0.24	-0.25	-0.19	0.29	0.41	0.53	0.48	12.24
<b>S7</b>	-0.21	-0.25	-0.17	0.30	0.43	0.55	0.53	11.61
<b>S8</b>	-0.22	-0.23	-0.20	0.28	0.44	0.52	0.55	11.05
<b>S9</b>	-0.20	-0.22	-0.16	0.26	0.43	0.55	0.54	10.33
<b>S10</b>	-0.20	-0.19	-0.19	0.27	0.43	0.52	0.54	9.76
<b>S11</b>	-0.21	-0.21	-0.18	0.28	0.33	0.43	0.55	NR
<b>S12</b>	-0.23	-0.20	-0.16	0.26	0.37	0.51	0.58	9.72
<b>S13</b>	-0.19	-0.20	-0.15	0.27	0.41	0.54	0.58	9.65
<b>S14</b>	-0.20	-0.19	-0.14	0.28	0.33	0.49	0.56	9.72
<b>S15</b>	-0.20	-0.22	-0.16	0.29	0.36	0.48	0.57	9.72
<b>S16</b>	-0.19	-0.20	-0.15	0.30	0.39	0.50	0.61	9.69
<b>S17</b>	-0.20	-0.20	-0.14	0.25	0.36	0.52	0.56	9.60
<b>S18</b>	-0.23	-0.19	-0.16	0.24	0.39	0.49	0.59	9.57
<b>S19</b>	-0.20	-0.19	-0.14	0.28	0.39	0.51	0.59	9.55
<b>S20</b>	-0.22	-0.21	-0.15	0.30	0.37	0.48	0.59	9.54
<b>Average</b>	-0.21	-0.21	-0.17	0.28	0.40	0.51	0.55	10.94

NR implies “not reliable” data

Table A.6 Mean free-surface elevation  $\bar{\eta}$  (cm) at 8 wave gauge locations, Test M1-M60

<b>Run</b>	<b>WG1</b>	<b>WG2</b>	<b>WG3</b>	<b>WG4</b>	<b>WG5</b>	<b>WG6</b>	<b>WG7</b>	<b>WG8</b>
<b>M1</b>	-0.20	-0.22	-0.28	0.22	0.35	0.46	0.56	8.77
<b>M2</b>	-0.24	-0.25	-0.23	0.28	0.38	0.48	0.55	8.46
<b>M3</b>	-0.20	-0.20	-0.17	0.28	0.37	0.51	0.57	8.43
<b>M4</b>	-0.22	-0.20	-0.17	0.29	0.40	0.53	0.52	8.36
<b>M5</b>	-0.19	-0.21	-0.18	0.24	0.39	0.46	0.57	8.34
<b>M6</b>	-0.20	-0.20	-0.17	0.29	0.40	0.48	0.47	8.62
<b>M7</b>	-0.22	-0.21	-0.17	0.30	0.40	0.54	0.59	8.65
<b>M8</b>	-0.22	-0.20	-0.17	0.25	0.37	0.47	0.57	8.62
<b>M9</b>	-0.21	-0.19	-0.16	0.28	0.34	0.50	0.57	8.73
<b>M10</b>	-0.24	-0.19	-0.17	0.25	0.34	0.48	0.55	8.71
<b>M11</b>	-0.24	-0.26	-0.18	0.24	0.38	0.41	0.50	9.29
<b>M12</b>	-0.20	-0.22	-0.16	0.26	0.37	0.47	0.49	8.72
<b>M13</b>	-0.21	-0.18	-0.16	0.30	0.40	0.57	0.51	8.80
<b>M14</b>	-0.23	-0.18	-0.15	0.32	0.41	0.50	0.50	8.75
<b>M15</b>	-0.19	-0.17	-0.15	0.28	0.36	0.53	0.52	8.70
<b>M16</b>	-0.20	-0.21	-0.15	0.31	0.40	0.51	0.48	8.70
<b>M17</b>	-0.19	-0.19	-0.14	0.28	0.36	0.47	0.50	8.65
<b>M18</b>	-0.23	-0.19	-0.15	0.28	0.40	0.51	0.52	8.54
<b>M19</b>	-0.21	-0.19	-0.15	0.30	0.32	0.53	0.49	8.66
<b>M20</b>	-0.23	-0.18	-0.17	0.29	0.39	0.48	0.51	8.66
<b>M21</b>	-0.26	-0.30	-0.22	0.26	0.29	0.45	0.55	9.13
<b>M22</b>	-0.27	-0.22	-0.17	0.30	0.31	0.46	0.56	8.59
<b>M23</b>	-0.21	-0.29	-0.16	0.28	0.35	0.48	0.56	8.54
<b>M24</b>	-0.23	-0.20	-0.16	0.28	0.31	0.46	0.55	8.68
<b>M25</b>	-0.22	-0.20	-0.15	0.28	0.36	0.49	0.56	8.67
<b>M26</b>	-0.19	-0.20	-0.15	0.28	0.32	0.46	0.58	8.59
<b>M27</b>	-0.19	-0.22	-0.13	0.32	0.37	0.48	0.57	8.60

<b>M28</b>	-0.18	-0.20	-0.18	0.29	0.29	0.50	0.56	8.58
<b>M29</b>	-0.22	-0.19	-0.15	0.28	0.29	0.48	0.56	8.57
<b>M30</b>	-0.22	-0.17	-0.13	0.30	0.37	0.53	0.62	8.55
<b>M31</b>	-0.19	-0.20	-0.21	0.25	0.32	0.41	0.48	9.19
<b>M32</b>	-0.22	-0.26	-0.21	0.28	0.33	0.48	0.53	8.53
<b>M33</b>	-0.21	-0.19	-0.15	0.32	0.39	0.53	0.53	8.51
<b>M34</b>	-0.22	-0.19	-0.15	0.32	0.32	0.47	0.55	8.60
<b>M35</b>	-0.21	-0.19	-0.15	0.31	0.33	0.46	0.55	8.52
<b>M36</b>	-0.22	-0.19	-0.14	0.30	0.37	0.47	0.54	8.57
<b>M37</b>	-0.19	-0.19	-0.14	0.31	0.33	0.49	0.55	8.56
<b>M38</b>	-0.22	-0.19	-0.15	0.31	0.33	0.49	0.55	8.54
<b>M39</b>	-0.20	-0.22	-0.15	0.31	0.37	0.45	0.53	8.51
<b>M40</b>	-0.20	-0.20	-0.15	0.28	0.32	0.48	0.55	8.56
<b>M41</b>	-0.18	-0.21	-0.20	0.30	0.26	0.44	0.54	9.16
<b>M42</b>	-0.25	-0.25	-0.16	0.33	0.33	0.52	0.54	8.53
<b>M43</b>	-0.22	-0.24	-0.21	0.30	0.34	0.49	0.51	8.64
<b>M44</b>	-0.17	-0.18	-0.15	0.30	0.38	0.50	0.59	8.67
<b>M45</b>	-0.22	-0.17	-0.15	0.34	0.34	0.51	0.59	8.67
<b>M46</b>	-0.22	-0.18	-0.17	0.31	0.38	0.55	0.60	8.61
<b>M47</b>	-0.21	-0.19	-0.16	0.30	0.37	0.51	0.58	8.71
<b>M48</b>	-0.20	-0.18	-0.14	0.35	0.33	0.51	0.50	8.49
<b>M49</b>	-0.18	-0.19	-0.15	0.33	0.36	0.51	0.58	8.63
<b>M50</b>	-0.19	-0.19	-0.15	0.29	0.37	0.51	0.56	8.61
<b>M51</b>	-0.16	-0.18	-0.17	0.28	0.31	0.44	0.62	9.19
<b>M52</b>	-0.21	-0.18	-0.21	0.34	0.32	0.46	0.62	8.70
<b>M53</b>	-0.18	-0.21	-0.21	0.33	0.35	0.45	0.62	8.68
<b>M54</b>	-0.21	-0.20	-0.15	0.32	0.41	0.46	0.67	8.66
<b>M55</b>	-0.20	-0.19	-0.15	0.36	0.33	0.47	0.64	8.63
<b>M56</b>	-0.20	-0.18	-0.15	0.34	0.33	0.49	0.64	8.64
<b>M57</b>	-0.18	-0.19	-0.14	0.35	0.28	0.47	0.68	8.62

<b>M58</b>	-0.21	-0.20	-0.15	0.33	0.34	0.45	0.70	8.61
<b>M59</b>	-0.19	-0.20	-0.14	0.31	0.37	0.46	0.63	8.59
<b>M60</b>	-0.17	-0.24	-0.15	0.32	0.32	0.49	0.59	8.59
<b>Average</b>	-0.21	-0.20	-0.16	0.30	0.35	0.49	0.56	8.66

NR implies “not reliable” data

Table A.7 Free-surface standard deviation  $\sigma_\eta$  (cm) at 8 wave gauge locations, Test E1-E20

<b>Run</b>	<b>WG1</b>	<b>WG2</b>	<b>WG3</b>	<b>WG4</b>	<b>WG5</b>	<b>WG6</b>	<b>WG7</b>	<b>WG8</b>
<b>E1</b>	4.89	4.92	4.78	3.50	3.00	2.78	NR	1.33
<b>E2</b>	5.04	5.07	4.90	3.54	3.03	2.80	NR	1.35
<b>E3</b>	5.08	5.11	4.94	3.52	3.03	2.78	NR	1.35
<b>E4</b>	5.10	5.11	4.95	3.57	3.02	2.77	NR	1.33
<b>E5</b>	5.09	5.11	4.93	3.55	3.02	2.80	NR	1.34
<b>E6</b>	5.09	5.12	4.94	3.55	3.03	2.78	NR	1.34
<b>E7</b>	5.09	5.11	4.94	3.56	3.04	2.80	NR	1.34
<b>E8</b>	5.08	5.12	4.93	3.54	3.01	2.79	NR	1.33
<b>E9</b>	5.08	5.11	4.92	3.52	3.02	2.79	NR	1.32
<b>E10</b>	5.08	5.10	4.92	3.53	3.03	2.78	NR	1.35
<b>E11</b>	4.84	4.90	4.80	3.47	2.98	2.71	NR	1.26
<b>E12</b>	5.01	5.05	4.94	3.52	3.00	2.75	NR	1.26
<b>E13</b>	5.07	5.12	4.99	3.53	3.00	2.75	2.33	1.32
<b>E14</b>	5.09	5.13	5.00	3.53	3.00	2.73	2.36	1.28
<b>E15</b>	5.09	5.13	5.00	3.54	3.03	2.75	2.34	1.29
<b>E16</b>	5.09	5.14	5.00	3.54	3.03	2.74	2.35	1.25
<b>E17</b>	5.09	5.12	4.99	3.53	3.03	2.74	2.36	1.29
<b>E18</b>	5.08	5.14	4.99	3.54	3.01	2.74	2.36	1.28
<b>E19</b>	5.09	5.13	4.98	3.53	3.03	2.75	2.34	1.26
<b>E20</b>	5.10	5.13	4.97	3.53	3.00	2.75	2.33	1.26
<b>Average</b>	5.06	5.09	4.94	3.53	3.02	2.76	2.35	1.31

\*NR implies “not reliable” data

Table A.8 Free-surface standard deviation  $\sigma_\eta$  (cm) at 8 wave gauge locations, Test S1-S20

<b>Run</b>	<b>WG1</b>	<b>WG2</b>	<b>WG3</b>	<b>WG4</b>	<b>WG5</b>	<b>WG6</b>	<b>WG7</b>	<b>WG8</b>
<b>S1</b>	5.00	5.05	4.91	3.50	2.98	2.78	2.09	NR
<b>S2</b>	5.05	5.13	4.98	3.49	3.03	2.79	2.02	1.48
<b>S3</b>	5.06	5.13	4.98	3.49	3.05	2.77	1.99	1.47
<b>S4</b>	5.06	5.13	4.98	3.48	3.03	2.77	2.00	1.47
<b>S5</b>	5.06	5.14	4.97	3.45	3.04	2.74	1.98	1.47
<b>S6</b>	5.06	5.11	4.95	3.48	3.03	2.74	1.97	1.45
<b>S7</b>	5.07	5.13	4.96	3.47	3.03	2.75	1.97	1.43
<b>S8</b>	5.03	5.11	4.94	3.48	3.02	2.75	1.95	1.42
<b>S9</b>	5.04	5.11	4.94	3.45	3.04	2.75	1.97	1.43
<b>S10</b>	5.05	5.12	4.92	3.45	3.03	2.75	1.95	1.44
<b>S11</b>	4.93	4.97	4.87	3.47	3.00	2.75	2.61	1.48
<b>S12</b>	5.02	5.05	4.94	3.46	3.01	2.75	2.59	1.47
<b>S13</b>	5.04	5.07	4.95	3.50	3.01	2.76	2.63	1.47
<b>S14</b>	5.06	5.09	4.96	3.46	3.01	2.76	2.61	1.48
<b>S15</b>	5.04	5.08	4.96	3.46	3.01	2.77	2.59	1.47
<b>S16</b>	5.05	5.09	4.96	3.46	3.02	2.77	2.61	1.49
<b>S17</b>	5.05	5.07	4.95	3.45	3.02	2.76	2.62	1.46
<b>S18</b>	5.04	5.06	4.95	3.46	2.99	2.76	2.61	1.49
<b>S19</b>	5.04	5.07	4.95	3.46	3.00	2.75	2.59	1.48
<b>S20</b>	5.02	5.05	4.93	3.47	3.01	2.77	2.59	1.48
<b>Average</b>	5.04	5.09	4.95	3.47	3.02	2.76	2.30	1.46

\*NR implies “not reliable” data

Table A.9 Free-surface standard deviation  $\sigma_\eta$  (cm) at 8 wave gauge locations, Test M1-M60

<b>Run</b>	<b>WG1</b>	<b>WG2</b>	<b>WG3</b>	<b>WG4</b>	<b>WG5</b>	<b>WG6</b>	<b>WG7</b>	<b>WG8</b>
<b>M1</b>	4.89	4.91	4.80	3.39	2.84	2.66	2.55	1.37
<b>M2</b>	5.01	5.01	4.89	3.40	2.86	2.67	2.54	1.39
<b>M3</b>	5.01	5.02	4.90	3.38	2.86	2.68	2.54	1.41
<b>M4</b>	5.01	5.03	4.90	3.39	2.89	2.67	2.54	1.41
<b>M5</b>	5.02	5.03	4.90	3.41	2.90	2.67	2.54	1.44
<b>M6</b>	5.01	5.03	4.92	3.38	2.88	2.66	2.55	1.47
<b>M7</b>	5.01	5.03	4.90	3.38	2.88	2.67	2.53	1.46
<b>M8</b>	5.02	5.04	4.90	3.40	2.89	2.66	2.52	1.40
<b>M9</b>	5.02	5.04	4.90	3.40	2.91	2.67	2.54	1.40
<b>M10</b>	5.00	5.04	4.89	3.39	2.91	2.68	2.53	1.39
<b>M11</b>	4.96	4.96	4.85	3.38	2.92	2.69	NR	1.48
<b>M12</b>	5.03	5.02	4.91	3.41	2.94	2.68	NR	1.47
<b>M13</b>	5.04	5.05	4.93	3.43	2.95	2.71	NR	1.47
<b>M14</b>	5.05	5.06	4.91	3.39	2.96	2.71	NR	1.45
<b>M15</b>	5.06	5.05	4.91	3.42	2.96	2.70	NR	1.48
<b>M16</b>	5.07	5.06	4.92	3.42	2.95	2.70	NR	1.43
<b>M17</b>	5.05	5.06	4.91	3.40	2.98	2.70	NR	1.45
<b>M18</b>	5.06	5.06	4.91	3.41	2.95	2.68	NR	1.45
<b>M19</b>	5.06	5.06	4.91	3.43	2.95	2.70	NR	1.47
<b>M20</b>	5.06	5.06	4.91	3.41	2.96	2.71	NR	1.47
<b>M21</b>	4.83	4.88	4.77	3.36	2.95	2.70	2.27	1.49
<b>M22</b>	4.95	4.99	4.86	3.36	2.94	2.70	2.26	1.51
<b>M23</b>	4.94	4.99	4.86	3.35	2.95	2.70	2.26	1.51
<b>M24</b>	4.95	4.99	4.86	3.36	2.96	2.71	2.26	1.53
<b>M25</b>	4.95	5.00	4.86	3.36	2.95	2.70	2.28	1.56
<b>M26</b>	4.97	5.01	4.86	3.37	2.96	2.71	2.27	1.54
<b>M27</b>	4.98	5.01	4.87	3.35	2.96	2.71	2.29	1.53

<b>M28</b>	4.97	5.01	4.86	3.33	2.94	2.71	2.27	1.58
<b>M29</b>	4.97	5.02	4.86	3.35	2.97	2.73	2.29	1.54
<b>M30</b>	4.95	5.00	4.85	3.34	2.96	2.73	2.28	1.55
<b>M31</b>	4.87	4.90	4.80	3.30	2.97	2.70	2.55	1.58
<b>M32</b>	5.00	5.02	4.90	3.35	2.97	2.73	2.55	1.54
<b>M33</b>	5.02	5.05	4.93	3.37	2.99	2.73	2.55	1.54
<b>M34</b>	5.04	5.06	4.93	3.34	2.98	2.73	2.56	1.56
<b>M35</b>	5.03	5.06	4.93	3.36	2.98	2.73	2.55	1.57
<b>M36</b>	5.03	5.06	4.93	3.34	2.99	2.74	2.56	1.55
<b>M37</b>	5.04	5.06	4.92	3.35	2.98	2.72	2.54	1.59
<b>M38</b>	5.04	5.06	4.92	3.35	2.99	2.74	2.57	1.55
<b>M39</b>	5.03	5.05	4.92	3.37	2.99	2.72	2.55	1.55
<b>M40</b>	5.04	5.06	4.91	3.34	2.99	2.73	2.56	1.57
<b>M41</b>	4.87	4.87	4.80	3.32	2.97	2.71	2.70	1.54
<b>M42</b>	5.00	4.99	4.90	3.37	2.99	2.74	2.69	1.52
<b>M43</b>	5.01	5.00	4.92	3.33	2.98	2.73	2.69	1.53
<b>M44</b>	5.01	5.00	4.92	3.37	3.00	2.74	2.71	1.54
<b>M45</b>	5.01	5.01	4.92	3.35	3.01	2.74	2.69	1.59
<b>M46</b>	5.03	5.03	4.92	3.33	2.99	2.74	2.68	1.53
<b>M47</b>	5.02	5.01	4.91	3.35	2.99	2.77	2.67	1.55
<b>M48</b>	5.01	5.01	4.92	3.36	2.98	2.75	2.60	1.60
<b>M49</b>	5.01	5.02	4.92	3.33	3.01	2.76	2.33	1.53
<b>M50</b>	5.01	5.01	4.90	3.33	2.99	2.74	2.32	1.54
<b>M51</b>	4.85	4.89	4.78	3.30	2.99	2.75	2.41	1.54
<b>M52</b>	4.97	5.01	4.87	3.33	2.99	2.73	2.44	1.53
<b>M53</b>	4.99	5.04	4.89	3.32	3.00	2.74	2.44	1.53
<b>M54</b>	5.00	5.05	4.90	3.32	3.01	2.75	2.48	1.52
<b>M55</b>	5.00	5.05	4.90	3.32	3.00	2.75	2.49	1.52
<b>M56</b>	4.99	5.04	4.88	3.33	3.01	2.75	2.49	1.53
<b>M57</b>	4.99	5.03	4.88	3.31	3.00	2.75	2.52	1.55

<b>M58</b>	5.00	5.03	4.89	3.32	3.01	2.75	2.57	1.59
<b>M59</b>	4.99	5.03	4.88	3.31	3.00	2.76	2.47	1.60
<b>M60</b>	4.98	5.02	4.87	3.34	3.00	2.76	2.36	1.50
<b>Average</b>	5.00	5.02	4.89	3.36	2.96	2.72	2.49	1.51

\*NR implies “not reliable” data

Table A.10 Mean  $\bar{U}$  and standard deviation  $\sigma_U$  of measured cross-shore velocity  $U$ , Test E1-E20

Run	2D ADV at WG4		Red Vectrino at WG5		Blue Vectrino at WG6	
	$\bar{U}$ (cm/s)	$\sigma_U$ (cm/s)	$\bar{U}$ (cm/s)	$\sigma_U$ (cm/s)	$\bar{U}$ (cm/s)	$\sigma_U$ (cm/s)
<b>E1</b>	-5.42	19.48	-2.45	14.68	-2.85	16.59
<b>E2</b>	-7.30	19.65	-2.84	14.66	-3.07	16.65
<b>E3</b>	-6.80	19.76	-2.52	14.97	-3.01	16.52
<b>E4</b>	-7.51	19.79	-2.15	14.66	-2.96	16.45
<b>E5</b>	-7.78	19.77	-2.24	14.96	NR	NR
<b>E6</b>	-7.58	19.75	-2.37	14.94	-2.54	16.46
<b>E7</b>	-6.22	19.48	NR	NR	NR	NR
<b>E8</b>	-6.52	19.24	NR	NR	-2.95	16.54
<b>E9</b>	-7.10	19.11	-2.64	14.88	-3.18	16.47
<b>E10</b>	-6.09	19.34	NR	NR	-2.98	16.67
<b>E11</b>	NR	NR	-2.45	14.68	-2.85	16.59
<b>E12</b>	-7.93	19.36	-2.84	14.66	-3.07	16.65
<b>E13</b>	-6.55	19.14	-2.52	14.97	-3.01	16.52
<b>E14</b>	-7.04	19.11	-2.15	14.66	-2.96	16.45
<b>E15</b>	-7.44	19.06	-2.24	14.96	NR	NR
<b>E16</b>	-7.44	18.92	-2.37	14.94	-2.54	16.46
<b>E17</b>	-6.56	18.76	NR	NR	NR	NR
<b>E18</b>	-6.65	18.63	NR	NR	-2.95	16.54
<b>E19</b>	-7.19	18.84	-2.64	14.88	-3.18	16.47
<b>E20</b>	-6.87	19.07	NR	NR	-2.98	16.67
<b>Average</b>	-6.95	19.28	-2.46	14.82	-2.94	16.54

NR implies 'Not reliable'.

Table A.11 Mean  $\bar{U}$  and standard deviation  $\sigma_U$  of measured cross-shore velocity  $U$ , Test S1-S20

Run	2D ADV at WG4		Red Vectrino at WG5		Blue Vectrino at WG6	
	$\bar{U}$ (cm/s)	$\sigma_U$ (cm/s)	$\bar{U}$ (cm/s)	$\sigma_U$ (cm/s)	$\bar{U}$ (cm/s)	$\sigma_U$ (cm/s)
<b>S1</b>	-5.88	18.84	-2.58	15.42	-2.43	17.03
<b>S2</b>	-8.64	18.85	-2.74	14.79	-3.18	16.69
<b>S3</b>	-7.78	18.94	-2.90	14.97	-3.14	16.62
<b>S4</b>	-6.84	18.81	-2.42	15.14	-3.35	16.68
<b>S5</b>	-6.67	18.88	NR	NR	-3.01	16.61
<b>S6</b>	-5.64	18.81	-2.88	15.23	NR	NR
<b>S7</b>	-7.46	18.91	-3.15	15.23	-3.20	16.65
<b>S8</b>	-7.70	18.78	-3.50	15.26	-2.96	16.45
<b>S9</b>	-6.39	18.67	-3.09	15.28	NR	NR
<b>S10</b>	-7.76	18.66	-2.78	15.26	-2.53	16.57
<b>S11</b>	-5.57	18.78	NR	NR	-2.53	16.53
<b>S12</b>	-6.26	18.80	NR	NR	-2.74	16.69
<b>S13</b>	-6.55	18.74	NR	NR	-2.51	16.37
<b>S14</b>	-6.81	18.71	NR	NR	-2.86	16.40
<b>S15</b>	-7.03	18.81	NR	NR	-2.82	16.49
<b>S16</b>	-6.65	18.75	-2.99	15.11	-2.58	16.42
<b>S17</b>	-5.67	18.96	NR	NR	-2.90	16.44
<b>S18</b>	-6.82	18.83	-2.89	15.01	-3.27	16.44
<b>S19</b>	-6.55	18.68	-2.95	14.88	-3.16	16.44
<b>S20</b>	-5.85	18.99	-2.41	15.11	-3.12	16.26
<b>Average</b>	-6.73	18.81	-2.87	15.13	-2.91	16.54

NR implies 'Not reliable'.

Table A.12 Mean  $\bar{U}$  and standard deviation  $\sigma_U$  of measured cross-shore velocity  $U$ , Test M1-M60

Run	2D ADV at WG4		Red Vectrino at WG5		Blue Vectrino at WG6	
	$\bar{U}$ (cm/s)	$\sigma_U$ (cm/s)	$\bar{U}$ (cm/s)	$\sigma_U$ (cm/s)	$\bar{U}$ (cm/s)	$\sigma_U$ (cm/s)
<b>M1</b>	-6.75	17.84	-2.32	14.28	-2.88	15.60
<b>M2</b>	-7.19	17.85	-2.82	14.25	-3.05	15.60
<b>M3</b>	-7.55	18.09	-2.22	14.38	-3.50	15.83
<b>M4</b>	-7.45	17.96	NR	NR	-2.85	15.74
<b>M5</b>	-6.22	17.97	-2.48	15.04	-2.70	15.69
<b>M6</b>	-7.09	18.08	-3.16	15.04	-2.88	15.63
<b>M7</b>	-7.03	18.18	-2.95	14.99	-2.76	15.81
<b>M8</b>	-6.90	18.15	-2.23	15.00	-3.12	15.92
<b>M9</b>	-7.53	18.07	-2.15	15.01	-3.04	15.87
<b>M10</b>	-6.66	18.11	-2.93	15.14	-2.97	15.96
<b>M11</b>	-5.71	17.84	-2.50	14.98	-3.16	15.27
<b>M12</b>	-7.41	17.84	-2.77	14.81	-3.42	15.12
<b>M13</b>	-6.49	18.05	NR	NR	-3.44	15.17
<b>M14</b>	-6.05	18.16	-2.29	15.11	-3.43	15.19
<b>M15</b>	-5.83	17.89	-2.63	15.06	-3.15	15.46
<b>M16</b>	-7.02	17.95	-2.25	14.93	-3.47	15.35
<b>M17</b>	-7.38	17.79	-2.87	14.95	-3.19	15.43
<b>M18</b>	-6.54	17.94	-2.93	14.97	-3.01	15.48
<b>M19</b>	-7.05	18.11	NR	NR	-2.95	15.54
<b>M20</b>	-7.02	17.91	NR	NR	-2.81	15.57
<b>M21</b>	-5.74	18.13	-1.92	12.07	-2.64	16.08
<b>M22</b>	-5.42	18.32	-1.88	11.75	-3.04	15.94
<b>M23</b>	-5.39	17.66	-1.68	11.84	-2.74	16.03
<b>M24</b>	-5.72	17.92	NR	NR	-2.95	16.12
<b>M25</b>	-6.44	17.71	NR	NR	NR	NR
<b>M26</b>	-5.25	17.84	-1.60	11.79	2.83	16.01

<b>M27</b>	-6.24	17.96	-1.69	12.09	NR	NR
<b>M28</b>	-6.20	17.75	-1.70	12.18	-2.80	16.16
<b>M29</b>	-5.87	17.99	-2.00	12.22	-3.20	16.20
<b>M30</b>	-6.16	17.61	-1.82	12.61	-2.82	16.13
<b>M31</b>	-6.28	17.74	-2.59	14.59	-2.76	15.75
<b>M32</b>	-6.30	17.93	-2.41	14.43	-2.74	15.81
<b>M33</b>	-6.65	17.85	-2.18	14.40	-2.60	15.76
<b>M34</b>	-6.12	17.61	NR	NR	NR	NR
<b>M35</b>	-5.57	17.86	-2.54	14.66	-2.87	15.88
<b>M36</b>	-6.63	17.76	NR	NR	-2.95	15.69
<b>M37</b>	-6.36	17.86	-2.17	14.68	-2.43	15.69
<b>M38</b>	-5.65	17.79	-2.03	14.60	-2.72	15.81
<b>M39</b>	-5.94	17.81	-2.10	14.31	-2.37	15.73
<b>M40</b>	-5.66	17.91	-2.13	14.38	-2.89	15.69
<b>M41</b>	-5.35	17.63	NR	NR	-2.27	15.67
<b>M42</b>	-6.00	17.79	-1.21	11.09	-2.99	15.79
<b>M43</b>	-6.03	17.90	-1.25	10.86	-3.01	15.85
<b>M44</b>	-5.74	17.56	NR	NR	-2.83	15.87
<b>M45</b>	-6.51	17.60	-1.69	11.23	-2.25	15.99
<b>M46</b>	-6.01	17.74	-1.43	11.07	-3.23	16.01
<b>M47</b>	-6.25	17.83	-1.32	10.86	-2.96	16.01
<b>M48</b>	-6.70	17.80	-1.09	10.45	-2.90	15.84
<b>M49</b>	-6.41	17.73	-1.14	10.35	-2.74	16.00
<b>M50</b>	-6.63	17.53	-1.06	10.83	-2.48	15.94
<b>M51</b>	-6.79	17.28	-1.26	10.74	-2.62	15.73
<b>M52</b>	-5.77	17.78	-0.95	10.40	-2.51	15.81
<b>M53</b>	-6.28	17.70	-1.09	10.86	NR	NR
<b>M54</b>	-6.88	17.56	-1.31	11.15	NR	NR
<b>M55</b>	-5.08	17.51	-1.17	11.40	NR	NR
<b>M56</b>	-6.54	17.84	-1.14	10.86	-2.48	15.91

<b>M57</b>	-6.15	17.70	-1.14	10.88	-2.42	15.89
<b>M58</b>	-6.21	17.42	-1.25	11.08	-2.39	15.80
<b>M59</b>	-6.08	17.48	-1.11	11.18	-2.56	15.83
<b>M60</b>	-5.04	17.75	-0.86	10.92	-2.51	15.80
<b>Average</b>	-6.32	17.83	-1.91	12.94	-2.75	15.77

NR implies 'Not reliable'.